Climate Linkers: Rationale and Pricing*

Pauline Chikhani[1] **and Jean-Paul Renne**[1,*]

[1]University of Lausanne, Faculty of Business and Economics (HEC), Department of Economics, Lausanne, CH-1015, SWITZERLAND
*Corresponding author; jean-paul.renne@unil.ch

ABSTRACT

This paper envisions climate linkers. We define climate linkers as long-dated financial instruments (bonds, swaps, and options) with payoffs indexed to climate-related variables, e.g., temperatures, sea levels, or carbon concentrations. On top of facilitating the sharing of long-term climate risks, another key benefit of these instruments would be informational, as their prices would reveal real-time market expectations regarding future climate. We develop and calibrate a sea-level-augmented integrated assessment model (IAM), and we exploit it to study climate-linked instruments' cost and risk characteristics. We examine, in particular, climate risk premiums: because of the insurance provided by a bond indexed on sea levels (say), investors would demand a lower average return on such a bond than on conventional bonds. Our findings highlight the sensitivity of climate premiums to the assumptions regarding (i) the damages associated with temperature increases and (ii) feedback effects between temperatures and carbon emissions.

Keywords: Integrated Assessment Model, Macroeconomic disasters, Climate derivatives, Term structure model, Social cost of carbon, Sea-level rise.
JEL codes: Q54, C32, E43, G12, H43.
Date: January 2022.

1 Introduction

The global annual average surface temperature has already increased by 1.1°C since 1880, intensifying the frequency and severity of adverse events—heatwaves, droughts, hurricanes, flooding. Extreme weather events are projected to worsen over the next century, as the global annual mean temperature increases. Through physical risks and transition risks (regulatory changes, technological innovations, and evolving consumer preferences), the medium- to long-term exposure of our economies to climate risk is considerable (e.g., Stern, 2007; Burke et al., 2015a,b; Dietz et al., 2016).

*We are grateful to Darrell Duffie, Adrian Fernandez-Perez, Elise Gourier, Christian Gouriéroux, Larry Kotlikoff, Hanno Lustig, Aleksandra Malova, Alain Monfort, Marcelo Ochoa, Riccardo Rebonato, Guillaume Roussellet, Patrick Saner, Simon Scheidegger, and Roméo Tédongap for useful comments. We also thank seminar participants at the 11th RCEA Money-Macro-Finance Conference, the 2021 ACFR-AUT Derivative Markets Conference, the 7th Annual Volatility Institute Conference at NYU Shanghai, the Federal Reserve Board Climate-related Risks, the Economy, and financial STability (CREST) virtual brown bag, McGill University, the ECON-GSW seminar, and the ACPR seminar. We hereby declare that we have no known competing financial interests or personal relationships that could have appeared to influence the work reported in this paper. R codes are available upon request.

In this paper, we envisions a novel class of financial instruments indexed to climate-related variables, such as global temperatures, carbon concentrations, or sea levels.[1,2] These instruments would not directly contribute to the fight against climate risks, in the sense that they do not necessarily aim at funding mitigation or adaptation projects (contrary to green bonds, e.g., Baker et al., 2018). They would, instead, serve three main purposes. First, they would facilitate the sharing of (physical) long-term climate risks. They would notably constitute an alternative and complementary sources of reinsurance capacity to support the insurance industry's goals in offering protection, as well as in providing direct capacity to those seeking to transfer long-term climate-related exposure. Second, the existence of a novel market for climate risks may stimulate investors to better understand climate risks, and incorporate them in their analyses.[3] Third, they would offer a public good by making market participants reveal their expectations regarding future climate. This information would be captured in real-time, at high frequency. One could for instance extract expected trajectories of future temperatures from market quotes of temperature-indexed swaps or bonds—in the same manner as inflation expectation measures are currently extracted from inflation linkers.[4] This would provide, in particular, a natural way to gauge the perceived credibility and effectiveness of international commitments regarding the climate.

The contribution of this paper is threefold. First, we discuss the advantages of financial instruments indexed to secular climate changes. Second, we develop a modeling framework that allows for the fast pricing of long-term financial instruments. Whereas it captures complex interactions between climate and macroeconomic variables, our Integrated Assessment Model (IAM) is solved instantaneously and offers quasi-analytical pricing formulas for swaps, bonds, and options indexed to sea levels, temperatures, or carbon concentrations, for any maturity. (To our knowledge, this paper is, in particular, the first to provide simple formulas to price of long-term bonds in an IAM framework.) Equipped with this model, we explore the pricing of climate linkers, which constitutes our third contribution.

Exploiting our analytical framework, we examine how linkers' prices would be affected by climate

[1] A market for weather derivatives already exists (Cao and Wei, 2004; Campbell and Diebold, 2005; Brockett et al., 2005). Pérez-González and Yun (2013) show that weather-sensitive firms have benefited from their introduction. To date, instruments traded on weather-derivative markets feature short time horizons (typically a few months) and focus on specific regional areas. In contrast, the derivatives discussed in this paper are long-dated and pertain to global risks. The long-dated nature of these instruments (and the resulting counterparty risks) would call for appropriate credit-mitigation mechanisms.

[2] Sea level rise stands as one of the most critical climate change's dangers (see, e.g., Hauer et al., 2016; Desmet et al., 2021, for evaluations of associated costs).

[3] Deficiencies in this area are studied by Davies et al. (2014) and Slawinski et al. (2017). In particular, standard insurance models remain rooted in the past, or backward-looking, and do not appropriately capture increasing climate-related risks (e.g., Bolton et al., 2020; Monasterolo, 2020; Swiss Re Institute, 2020). Recent studies however suggest that bond markets have become sensitive to climate-related considerations (e.g. Cevik and Jalles, 2020). Relatedly, climate vulnerability is now taken into account by credit rating agencies (Standard & Poor's Global, 2017). Krueger et al. (2021) provide survey-based evidence of an increase in climate-risk perceptions by institutional investors.

[4] Relatedly, extreme temperature scenarios could be derived from market prices of temperature options. These scenarios would, in particular, be useful to design climate stress tests (Battiston et al., 2017). They would reflect risk-adjusted trajectories of climate variables; risk premiums should be extracted from option prices to reflect physical trajectories. (The risk premium extraction can be based on a model such as the one presented in the present paper.)

risk premiums. These premiums are defined as the price components arising because agents are averse to climate risks (Dietz et al., 2018; Lemoine, 2021). Our model recognizes that, for a given expected payoff, agents favor assets that tend to provide larger payoffs in "bad states of the world," which correspond here to situations where realized temperatures are above their expected trajectory. Consider, for instance, a 50-year temperature-indexed bond (TIB) whose repayment value increases by 10% if atmospheric temperature is 0.1°C higher than expected at maturity. Our results find that the associated yield-to-maturity would be 25 basis points lower than that of a standard (50-year) zero-coupon bond providing the same expected payoff. This is because this TIB embeds insurance against increasing temperatures, implying that investors are willing to hold these bonds even if their expected return is lower than for standard ones.

We further examine the importance of climate-risk premiums in long-dated temperature options. We focus on digital options, whose payoff is equal to one if the atmospheric temperature exceeds a given value—the option strike—and zero otherwise. The price of such an option can be interpreted as the risk-adjusted probability of the temperature exceeding the strike. (Interestingly, one could use the prices of options of strike 2°C to measure the benefits associated with achieving the objectives of the Paris agreement.) Our results show that for high-temperature strikes and long horizons—a temperature anomaly of 3°C, say, and horizons between 50 and 100 years— risk-adjusted probabilities can be several times larger than physical ones. We also find that this ratio positively depends on the strike. This result is reminiscent of those obtained in the literature on disaster-risk pricing: risk premiums represent the bulk of the prices of those financial instruments providing larger payoffs in disastrous situations (financial meltdowns, defaults of large corporate or sovereign entities, see, e.g., Elton et al., 2001; Coval et al., 2009).

This research relates to the literature investigating the pricing of climate risks. A large share of the theoretical literature is concerned with the computation of the Social Cost of Carbon (SCC), defined as the marginal value of emission reductions (e.g., Weitzman, 2013). Uncertainty and aversion to ambiguity are found to have profound implications on the SCC calculations (e.g., Daniel et al., 2019; Cai and Lontzek, 2019; Barnett et al., 2020; Lemoine, 2021; van den Bremer and van der Ploeg, 2021). While the present paper focusses on the pricing of fixed-income instruments, we also examine the SCC resulting from our model. Our SCC estimate is $167 per ton of carbon, which stands among the highest values found in the literature.

The empirical literature on the pricing of climate risks in financial products is rapidly growing. Several articles assess the relative value of green or environmental, social, and governance (ESG) bonds, pointing to small premiums to otherwise similar ordinary bonds (Baker et al., 2018; International Monetary Fund, 2019; Larcker and Watts, 2020). Other studies look for market price evidence of climate risk premiums: Huynh and Xia (2020) find that corporate bonds whose value tend to increase when bad news about the climate occur trade at a premium; Painter (2020) shows that long-dated municipal bond yields are higher for counties with large expected losses due to sea level rise. Since investors have been considering

climate risk for a relatively short period of time, quantitative estimates of climate risk premiums based on (short) historical samples should be taken with caution (Giglio et al., 2020). After having constructed a climate-news index, Engle et al. (2020) propose an approach to dynamically hedging the associated risks using stocks-based factor-mimicking portfolios. Andersson et al. (2019) show that one can closely track leading equity indices with portfolios featuring a carbon footprint 50% smaller than the benchmark.

The present paper is particularly close to those studies that investigate asset pricing in the context of stochastic integrated assessment models (IAMs). In this literature, some studies rely on models whose tractability is obtained by simplifying the climate block of the Dynamic Integrated Climate-Economy model (DICE) of Nordhaus (1992) (e.g. Bansal et al., 2016; Karydas and Xepapadeas, 2019; Bansal et al., 2019). Other studies employ standard DICE-related IAMs and look for efficient pricing solutions (e.g., Daniel et al., 2019; Barnett et al., 2020). We manage to combine approximate DICE-type equations and closed-form pricing solutions. This is achieved by making the state variables' dynamics depend on combinations of deterministic and stochastic components. As in Traeger (2021), the stochastic components are such that the conditional Laplace transform of the state vector is affine in its past values—in a time-dependent but deterministic fashion.[5] The model tractability hinges on the properties of affine processes (see, e.g., Duffie, 1996; Duffie et al., 2003; Piazzesi, 2010). Equipped with closed-form formulas for expectations and covariances of the state variables—at any horizon—we propose an original calibration approach to make the model replicate benchmark scenarios and outputs of reference climate models.[6,7] This calibration approach is infeasible in the context of standard IAMs, whose resolution is not immediate.

The remainder of this paper is organized as follows. In Section 2, we expose the rationale behind climate linkers. Section 3 details how these derivatives could be structured; it also discusses the concept of climate risk premiums. Section 4 outlines our modeling framework, and Section 5 discusses its implications in terms of climate derivatives' pricing. Section 6 concludes. Technical details are gathered in Appendices A (model) and B (calibration). All pricing formulas are given in the online appendices (page 42).

[5] In spirit, this approach is similar to the one underlying the so-called market models of interest rates (Brace et al., 1997; Miltersen et al., 1997).

[6] The model resolution and price calculation run several orders of magnitude faster than those based on dynamic programming approaches (Cai and Judd, 2014; Cai and Lontzek, 2019; Barnett et al., 2020). For the latter approaches, solving for the model on a single set of parameters is not fast enough to allow for a calibration approach that necessitates solving the model a large number of times.

[7] No grid-based approach—subject to the curse of dimensionality—is needed to solve the model. By way of comparison, Daniel et al. (2019) employ their approximated solution method in a context where both the number of dates and the number of states are small (seven dates are considered, from 2015 to 2400; each node is followed by two possible states, leading to 2^7 possible states in 2400, and only 4 in 2100).

2 Rationale behind climate-linkers

2.1 Hedging demand

In the coming decades, the frequency and severity of weather and climate disasters will increase, pushing insurance and reinsurance claims up. According to the Swiss Re Institute (2020), total economic losses from weather-related catastrophes amounted to $1'600bn between 2010 and 2019, 60% higher than 2000-2009, and 100% higher than for 1990-1999. Moreover, hedging needs are likely to increase to close the so-called insurance gap—the difference between insured and total losses (Batten et al., 2016; Wolfrom and Yokoi-Arai, 2016). This gap has widened over time in absolute terms, as the substantial growth in insurance penetration was not significant enough to keep up with the increase in weather-related losses.

Growing demand for insurance against weather-related disasters has led to the emergence of alternative risk transfer solutions (ART), such as insurance-linked securities (ILS), among which stand catastrophe bonds and the so-called sidecars (special-purpose reinsurance vehicles). Insurers typically use ILS as an alternative to traditional catastrophe reinsurance (Charpentier, 2008; Cummins and Weiss, 2009). While these instruments add to the capacity of the insurance sector to deal with natural catastrophes, they do not protect against long-term climate risks. Indeed, climate change is a slow-moving and long-term phenomenon. In contrast, ILS are typically short-term instruments: Most catastrophe bonds have a term of three years, and private transactions linked to natural catastrophe risk typically provide cover for 12 months (Cummins and Weiss, 2009). Over such horizons, climate change is essentially predictable, and the risk level of an ILS does not change between inception and redemption. As a result, these instruments do not help transfer risks associated with long-term climate change effects. This may contribute to the moderate appetite for this kind of bonds.[8] The demand for catastrophe bonds also suffers from their relative illiquidity—the risk covered by each being very specific (in the peril and geographical dimensions).

Unlike existing ILS, the instruments discussed in this paper would allow for the transfer of long-term climate-related risks. They could benefit the (re)insurance industry by helping them cope with worse-than-expected long-term scenarios.[9] They would also provide new perspectives of diversification to long-term investors such as pension funds. A recent renewed interest in century bonds is suggestive of an increasing appetite for ultra-long-term bonds.[10]

It is important to note that these instruments would be fundamentally different from green or environ-

[8] The relative cheapness of these bonds is illustrated by the fact that spreads for catastrophe bonds are substantially larger than similarly-rated corporate high-yield debt and are typically four times larger than expected losses (Braun, 2016). Note that the rating of catastrophe bonds is low (typically BB) because the probability of incurring large losses is high.

[9] Mills (2005) describes the long-run difficulties that an adverse climate scenario would pose to the insurance industry.

[10] Austria issued a 100-year bond in 2017 and 2019, raising EUR 4.75 billion. Long-dated debt is attractive to institutional investors like pension or mutual funds looking for investments to match long-term liabilities and hedge funds seeking to make gains through currency or interest rate swap trades. What makes them specific is a high convexity—a measure of the curvature of the relationship between bond prices and bond yields. A high-convexity bond is such that a one-unit increase in the yield-to-maturity results in a bond price decrease that is lower than the price increase following a one-unit drop in interest rates. In other words, a high-convexity bond is a good hedge against falling yields.

mental, social, and governance (ESG) fixed-income products. The latter are instruments to fund projects that have a positive environmental and/or climate impact; they are the building blocks of sustainable finance, defined as the process of taking into account environmental and social considerations in investment decision-making (Baker et al., 2018; International Monetary Fund, 2019; Larcker and Watts, 2020; Hong et al., 2020). Nevertheless, since the payoffs of standard ESG bonds are not state-dependent, these products do not directly allow for the transfer of climate-related risks.[11]

2.2 The supply side

Governments constitute potential issuers of climate-indexed debt instruments. Following the global financial crisis and the Covid19 pandemic, governments worldwide have been facing important funding needs. Thus, issuing novel types of bonds may support the demand for sovereign debt by widening the investor basis. Importantly, contrary to green bonds (or, more generally, ESG bonds), the proceeds of climate-indexed bonds do not necessarily have to be invested in environment-related projects. In other words, the issuance of climate-indexed bonds would not interfere with climate and environmental policies pursued by governments; these novel debt instruments would complement existing ones (i.e., nominal and inflation-indexed bonds).

All else being equal, by issuing climate-indexed bonds—with payoffs that positively depend on temperature (say)—governments would increase their long-term exposure to climate risks. Notwithstanding substantial international coordination problems, this would strengthen their incentives to implement policies fighting these long-term risks. It can be noted here that governments already provide climate-risk hedging as "insurers of last resort" (Bruggeman et al., 2010). In several countries, government (re)insurance facilities have been established to support insurance availability. These facilities provide direct insurance to property owners for disaster risks or provide reinsurance coverage to insurance companies for such risks (Wolfrom and Yokoi-Arai, 2016).[12] In many countries, such facilities specifically aim at reducing the maximum risk exposure faced by the insurance sector in the event of a disaster, thereby addressing a key criterion for insurability (Berliner, 1985).[13] By increasing their exposure to climate risk, governments would also have more incentive to implement policies fighting it.

By providing insurance to bondholders through the issuance of climate-indexed bonds, governments

[11] A derivatives market associated with ESG products is developing (Lannoo and Thomadakis, 2020); the first ESG-linked sustainability-improvement derivative was issued in 2019. As the underlying ESG bonds, these derivatives do not provide (direct) insurance against climate risk; instead they allow to hedge against the risk associated with those investments taking ESG criteria into consideration.

[12] Examples of comprehensive direct insurance facilities include the Consorcio de compensacion de seguros in Spain, and Iceland Catastrophe Insurance. Direct insurance is also provided by the New Zealand Earthquake Commission, the Turkish Catastrophe Insurance Pool and the United States National Flood Insurance Program, although for a sub-set of disaster risks. Examples of reinsurance facilities include the Caisse centrale de réassurance in France (for all disaster risks), and Japan Earthquake Reinsurance for a smaller sub-set of risks.

[13] Charpentier and Le Maux (2014) study the conditions under which reinsurance of natural catastrophe risks by the government improves welfare.

may expect to earn climate-risk premiums when issuing such instruments. Because these assets would deliver higher payoffs in "bad states of nature"—characterized by higher marginal utility of consumption—investors should indeed be willing to buy these bonds even if their expected returns are lower than those of standard bonds (with fixed payoffs). That is, as of the date of issuance, the government should expect these issuances to eventually result in lower debt service. This has been one of the arguments in favour of the issuance of inflation-indexed bonds (see, e.g., Price, 1997, Section II.B). There are however two caveats to this line of reasoning. The first is that the premium would probably be reduced—if not canceled—in the early years, due to the existence of a negative "novelty premium"; empirical evidence indeed suggests that investors tend to ask for premiums to hold new types of asset.[14] The second, more theoretical, is that it is not clear that public debt managers should take the minimization of the average cost of debts as their main target; instead, borrowing costs must be considered in relation to risk (Campbell and Shiller, 1996, Section 2).[15]

By reducing entry costs—materializing through the novelty premium mentioned above—the issuance of sovereign climate-indexed bonds could open the door to private issuances and promote the development of a liquid market.[16] From an asset-liability management perspective, natural issuer candidates would be firms whose activity relates to climate-risk mitigation (e.g., renewable-energy producers and electric-vehicle makers). More generally, the introduction of sovereign climate-indexed bonds would contribute to the development of climate derivatives markets. In this respect, the development of the market of inflation-indexed derivatives stands as an example: Following the introduction of U.S. government inflation-linked bonds, the Chicago Board of Trade introduced futures and options referenced to these bonds; mutual funds benchmarked on these bonds also developed, and inflation-linked investment plans and annuities were introduced by pension funds (García and Van Rixtel, 2007).

2.3 Informational content

The benefits expected from the development of climate-indexed instruments are also informational. Indeed, the prices of climate-indexed instruments would reflect the market expectations regarding the future trajectory of climate-related variables (e.g., temperatures, carbon concentrations). Furthermore, if climate options were traded, one could also back out measures of the perceived uncertainty associated with these expected trajectories.

[14] The novelty premium can reflect potential difficulties in measuring the risks underlying the asset (e.g. due to the absence of appropriate and well-established models) or the limited liquidity of such bonds relative to conventional ones. Employing a no-arbitrage term-structure model, D'Amico et al. (2018) find for instance that inflation-linked bond yields exceeded risk-free real rates by as much as 100 basis points when they were first issued in the U.S..

[15] Such a cost-risk trade-off seem to be consistent with the actual public debt management practices. Indeed, if governments were essentially minimizing borrowing costs, then they would massively borrow at the Treasury bill rate and would invest the proceeds in longer-term bonds (thereby earning the term premium) or in stock markets (thereby earning the equity premium).

[16] As Campbell and Shiller (1996, p.191) put it: "It is widely acknowledged that the proper role of the government is to provide public goods, and the demonstration by example of the potential for new financial markets and instruments is really a public good."

These expectations and trajectories would be adjusted for risk: expectations that are extracted from market prices embed risk premiums and therefore do not necessarily coincide with physical expectations of future climate.[17] However, as long as the risk premium components of climate-linkers' prices vary relatively slowly through time, changes in climate linkers may still be interpreted as changes in expectations. Moreover, models—such as the one presented in Section 4—could be used to try and extract risk premiums from observed market prices to recover corrected (physical) expectations.

Naturally, such market-based measures would not, per se, improve our understanding of climate change. Having the market reveal their expectations would however be valuable in several respects. First, to price these instruments, market participants would develop and employ climate models, which would contribute to research efforts on climate modeling.[18,19] Second, the observation of changes in these prices (available at high frequency) would allow measuring the influence of different types of news on agents' expectations. Typically, one could observe how markets evaluate the effectiveness of policies announced during international summits.[20,21] In particular, one could observe whether the objectives of the Paris agreement of 2015—holding the global average temperature below 2°C above pre-industrial levels—is deemed credible by market participants.

Third, the trajectories of climate-related variables backed out from observed prices (temperatures, say, in the case of temperature-indexed bonds) may be used to construct "market-based" scenarios. These scenarios would complement model-based ones and may be used, e.g., to price long-term insurance premiums or assets exposed to climate risks. Importantly, if climate options were available, the definition of worst-/best-cased scenarios (corresponding to specific probabilities) could also be derived. The latter may for instance help design climate stress tests (Battiston et al., 2017; Bolton et al., 2020).

3 Climate linkers

This section introduces different types of climate linkers. While we focus on derivatives whose payoffs depend on a temperature index, different climate-related indices could be considered. In particular, we could replace temperature indices with measures of sea level or carbon concentration (as is illustrated in

[17] As an example, in the context of the term structure of interest rates, empirical evidence suggests that forward rates do not coincide with the (physical) expectation of future interest rates. That is, the so-called "expectation hypothesis" does not hold (see, among many others, Cochrane and Piazzesi, 2005).

[18] According to the OECD, in 2017, the U.S. R&D spending in the finance and insurance sector amounted to $7.6bn, which compares, e.g., to $8.8bn for R&D expenditures in the chemical sector.

[19] Relatedly, Purnanandam and Weagley (2016) show that the introduction of weather derivatives by the Chicago Mercantile Exchange, in the late 1990s, has generated additional scrutiny of the temperature data.

[20] Central banks, academics, market analysts or practitioners widely resort to such approaches to assess the influence of announcements or news on inflation expectations (using inflation derivatives). Revealing inflation expectations was among the principal arguments for the development of inflation-indexed bond markets (see, e.g., Price, 1997).

[21] In this spirit, Gürtler et al. (2016) investigate how the occurrence of catastrophes lead market participants to reprice catastrophe bonds.

Subsection 5.3).[22]

For expository purpose, we abstract from inflation. It seems however appropriate to make climate linkers' payoffs indexed to inflation.[23] This way, these instruments would constitute pure hedges against physical climate risk, without being affected by inflation-risk premiums.

Let us start with the definition of a temperature-indexed swap. A swap is a basic derivative product that materializes the agreement between two counterparties to exchange cash flows at predetermined dates. The first type of the cash flows is determined at the time the swap is negotiated and paid by the protection buyer to the protection seller. The second type of cash flows depends on an index that is observed after the negotiation; these cash flows are paid by the protection seller to the protection buyer. In a Temperature Indexed Swap (TIS), the reference index is a temperature measure. This derivative would allow investors to either reduce or increase their exposure to climate change.

Definition 1. Temperature Indexed Swap (TIS). *A zero-coupon TIS is a derivative in which a fixed rate payment on a notional amount (N, say) is exchanged for a payment indexed to a given temperature measure (T_t, say).*[a]

Denote the current (negotiation) date by t. If the maturity date is $t+h$, then the temperature seller will pay $T_{t+h}N$ to the temperature buyer on date $t+h$ (this is the protection leg of the swap); and the latter gives $T^S_{t,h}N$ to the temperature seller (this is the premium leg of the swap). In other words, the protection buyer and seller respectively receive $(T_{t+h}-T^S_{t,h})N$ and $(T^S_{t,h}-T_{t+h})N$ on date $t+h$.

The temperature swap rate ($T^S_{t,h}$) is negotiated by the the two counterparties on date t; it is such that the values of the two legs are equal on date t.

[a] T_t here denotes a generic temperature measure. It could be the atmospheric temperature, the ocean temperature, or a combination of the two.

While the temperature swap rate ($T^S_{t,h}$) is negotiated on date t by the two counterparties, T_{t+h} is observed on date $t+h$ only. That is, while the value of the premium leg is known as of date t, this is not the case of the protection leg.

Let us take advantage of the simplicity of this instrument to introduce climate risk premiums. To start with, consider the baseline case where agents are risk-neutral and risk-free interest rates are independent

[22] In any case, the definition and calculation of the index should be precisely defined; in particular, the calculation should be based on perennial and reliable sources.

[23] For this, the payoffs given in Definitions 1, 2, and 3 would have to be multiplied by PI_{t+h}/PI_t, where PI_t denotes a price index prevailing on date t. In terms of pricing, the formulas developed in the Online Appendix III would remain valid under the assumption that the (log) inflation rate $\pi_{t,t+1} = \log(PI_{t+1}/PI_t)$ is an affine combination of the state vector components.

from temperatures. Under the absence of arbitrage opportunities, we then have:

$$T^S_{t,h} = \mathbb{E}_t(T_{t+h}), \tag{1}$$

where $\mathbb{E}_t$ denotes the expectation conditional on the information available on date t.

The protection buyers then receives $(T_{t+h} - \mathbb{E}_t(T_{t+h}))N$ at maturity. Thus, when temperature rises above its expected path, the temperature buyer receives more from the temperature seller than what he pays, and vice versa.

Let us now relax the risk-neutral assumption, and denote by $\mathscr{M}_{t,t+h}$ the stochastic discount factor (s.d.f.) between dates t and $t+h$.[24] Note that the s.d.f. considered here is general, and the formulas presented in this section are not specific to the modeling framework described in Section 4.

The price of the protection leg is $\mathbb{E}_t\left[T_{t+h}\mathscr{M}_{t,t+h}\right]$, and that of the premium leg is $T^S_{t,h}\mathbb{E}_t\left[\mathscr{M}_{t,t+h}\right]$. The fact that the two legs of the swap have the same value as of date t then gives:

$$T^S_{t,h} = \mathbb{E}_t\left[\frac{\mathscr{M}_{t,t+h}}{\mathbb{E}_t\left[\mathscr{M}_{t,t+h}\right]}T_{t+h}\right]. \tag{2}$$

The previous equation shows that the TIS rate can be seen as a risk-adjusted expectation of T_{t+h}, and that the risk-adjustment depends on $\mathscr{M}_{t,t+h}/\mathbb{E}_t\left[\mathscr{M}_{t,t+h}\right]$. Formally, $T^S_{t,h}$ is called h-forward risk-neutral expectation of T_{t+h}, and $\mathscr{M}_{t,t+h}/\mathbb{E}_t\left[\mathscr{M}_{t,t+h}\right]$ is the Radon-Nikodym derivative linking the physical and risk-neutral measures.[25]

Eq. (2) also rewrites

$$T^S_{t,h} = \mathbb{E}_t\left[T_{t+h}\right] + prem_{t,h}, \quad \text{with} \quad prem_{t,h} = \frac{\mathbb{C}ov_t\left[T_{t+h}, \mathscr{M}_{t,t+h}\right]}{\mathbb{E}_t\left[\mathscr{M}_{t,t+h}\right]}, \tag{3}$$

which shows that $prem_{t,h}$, the difference between the swap-implied temperature ($T^S_{t,h}$) and the expected temperature ($\mathbb{E}_t\left[T_{t+h}\right]$), depends on the covariance between temperatures and the s.d.f.: if states of higher temperature are perceived as "bad states of the world" (states of high marginal utility, or high s.d.f.) then the swap-implied temperature is above its expectation because the covariance term is then positive. In that case, the protection buyer is willing to lose money, on average, to be hedged against temperature risk.

In the context of the pricing model presented in Section 4, Corollary 3 of Appendix III enables the computation of the two conditional expectations appearing in eq. (2). (In particular, in this model, the

[24] In the discrete-time context, it can be shown that under the assumptions of (a) existence of a price, (b) price linearity and continuity and (c) absence of arbitrage opportunity, there exists a positive SDF. This derives from a conditional version of the Riesz representation theorem (see e.g. Hansen and Richard, 1987).

[25] The h-forward risk-neutral measure $\mathbb{Q}^h$ is equivalent (in the measure sense) to the physical one. Under $\mathbb{Q}^h$, the numeraire is a zero-coupon bond of maturity h (see e.g. Jamshidian, 1989). That is, conditional on the information available on date t, the risk-adjusted probability of an event Ω_{t+h} (say) is equal to $\mathbb{E}_t(\mathscr{M}_{t,t+h}\mathbb{1}_{\{\Omega_{t+h}\}})/\mathbb{E}_t(\mathscr{M}_{t,t+h})$.

s.d.f. $\mathscr{M}_{t,t+h}$ is available in closed form.)

Definition 2. Temperature Indexed Bond (TIB). *A zero-coupon TIB is a debt instrument whose payoff is indexed to a given measure of temperature. Let us denote by t the issuance date and by h the maturity at issuance. The payoff, settled on date $t+h$, is of the form:*

$$1+\chi(T_{t+h}-T^0_{t,h}), \tag{4}$$

where $T^0_{t,h}$ is a temperature defined by the issuer on the issuance date and where parameter χ is a "leverage factor." The temperature $T^0_{t,h}$ could for instance be set to the expected temperature on date $t+h$ (as of date t), that is $T^0_{t,h}=\mathbb{E}_t(T_{t+h})$. In that case, the expected payoff of the TIB would be equal to 1.

While the expected payoff of the TIB is equal to that of a standard zero-coupon bond when $T^0_{t,h}=\mathbb{E}_t(T_{t+h})$, the price of the two types of bonds (with matching maturities) are not necessarily equal. Formally, the TIB price is then given by:

$$\mathbb{E}_t\left[\mathscr{M}_{t,t+h}\{1+\chi(T_{t+h}-\mathbb{E}_t(T_{t+h}))\}\right] \quad = \quad \mathbb{E}_t\left[\mathscr{M}_{t,t+h}\right]+\chi\, prem_{t,h},$$

where $prem_{t,h}$ is defined in eq. (3). Therefore, the difference between the TIB price and $\mathbb{E}_t\left[\mathscr{M}_{t,t+h}\right]$—that is the price of a zero-coupon bond with a deterministic payoff of 1 at maturity—is equal to $\chi\, prem_{t,h}$.

It can be noted that the TIB payoff turns negative if $T_{t+h}<T^0_{t,h}-\frac{1}{\chi}$ (eq. (4)). To prevent this, TIBs could embed options for the payoff to be equal to $\max[1+\chi(T_{t+h}-T^0_{t,h}),0]$.[26] In the context of our pricing model, the TIB valuation formulas given in Corollary 4 of Appendix III would then have to be adjusted with option prices. We now introduce such options.

Definition 3. Temperature options. *A temperature option is a derivative instrument whose payoff is nonlinearly indexed to a given temperature measure. We consider three types of options:*

Option type	*Price (notation)*	*Payoff (settled on maturity date $t+h$)*
Digital	$Dig_{t,h}(T_K)$	$\mathbb{1}_{\{T_{t+h}>T_K\}}$
Call	$Call_{t,h}(T_K)$	$(T_{t+h}-T_K)^+=\mathbb{1}_{\{T_{t+h}>T_K\}}(T_{t+h}-T_K)$
Put	$Put_{t,h}(T_K)$	$(T_{t+h}-T_K)^-=\mathbb{1}_{\{T_{t+h}<T_K\}}(T_K-T_{t+h})$

[26] Relatedly, U.S. Treasury Inflation-Protected Securities (TIPS) embed a put option for the nominal redemption value to be higher than the original principal; this option hedges investors against deflation (see, e.g., Grishchenko et al., 2016).

A temperature call of strike 3°C allows, for instance, to get the payoff $(T_{t+h} - 3)$ on date $t+h$ if $T_{t+h} > 3$. Proposition 11 of Appendix III enables to price these options' in the context of the model presented in Section 4.

4 Model

This section presents a modeling framework that we will subsequently use to get insight into the pricing of the climate linkers introduced above. At the intersection between the well-known DICE model (Nordhaus, 2017) and the concise climate change economy of Bansal et al. (2019), the model offers closed-form solutions for pricing different classes of assets. As schematically represented in Figure 1, the model captures relationships between economic and climatic variables. In the remainder of this section, we highlight the fundamental equations and ingredients of the model. Appendix A depicts the full model.

Figure 1. Schematic representation of the model

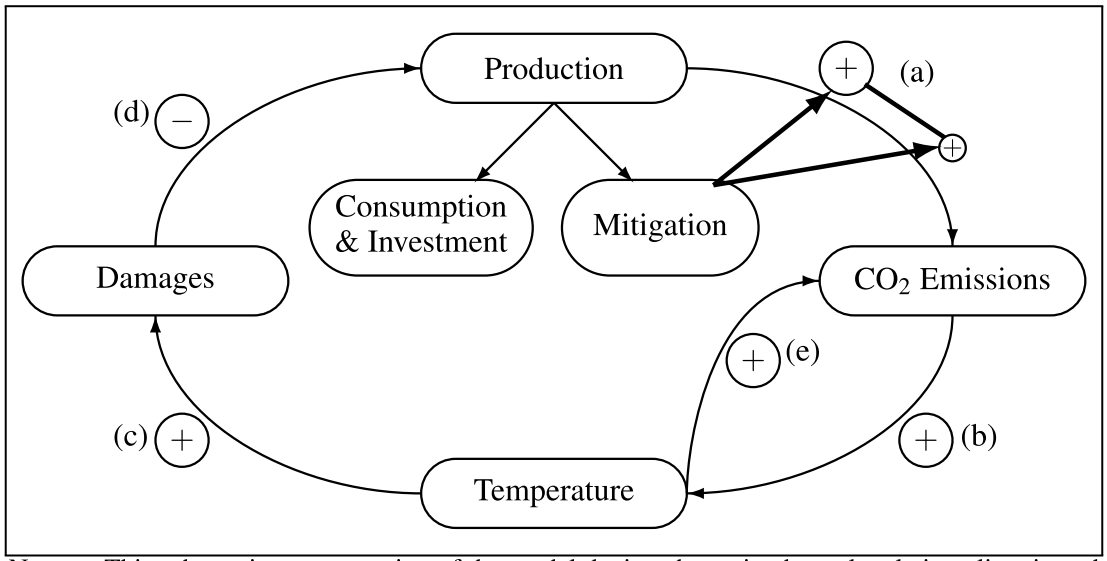

Note — This schematic representation of the model depicts the main channels relating climatic and economic variables. (a): Production increases emissions, but mitigation helps to reduce the positive relationship between the two. (b): Emissions increase temperature anomaly. (c): Larger temperatures increase the probability of agent's being hit by climate-driven damages. (d): Damages negatively impact production through a reduction in the quality of capital. (e): Temperature raises emissions by increasing the probability of triggering a climate change feedback loop (triggered, e.g., by releasing tons of methane trapped in the permafrost, or the acidification of oceans).

4.1 Climate block

In the model, temperatures are expressed as temperature anomalies from a baseline period.[27] As proposed in the DICE model, we focus on two global temperatures: lower ocean (T_{LO}) and atmosphere (T_{AT}). The dynamics of these two temperatures depends on radiative forcings due to greenhouse gases (F): Earth receives radiant energy from the Sun and emits some energy back into space; at equilibrium, Earth should absorb as much radiant energy as it radiates out of our atmosphere; the difference between the two is radiative forcings. When the latter goes up, absorption increases, and Earth warms. Specifically, the atmosphere temperature—which drives damages to the economy—is determined as follows:[28]

$$T_{AT,t} = T_{AT,t-1} + \xi_1 \left\{ F_t - \frac{\tau}{\nu} T_{AT,t-1} - \xi_2 \left[T_{AT,t-1} - T_{LO,t-1} \right] \right\}. \tag{5}$$

In the present model, we consider the following linear approximation to the dynamics of radiative forcings:

$$F_t = \tau \log_2(m_0) + \frac{\tau}{\log(2) m_0} \left(\frac{M_{AT,t}}{M_{PI}} - m_0 \right) + F_{EX,t} + \sigma_F \eta_{F,t}, \tag{6}$$

where $F_{EX,t}$ is the (exogenous) part of radiative forcings that is due to non-CO_2 greenhouse gases,[29] $M_{AT,t}$ is the mass of carbon in the atmosphere, and M_{PI} is its preindustrial level. Moreover, m_0 is the value of $\frac{M_{AT,t}}{M_{PI}}$ at which the linearization is performed. Online Appendix IV.1 demonstrates that the previous first-order approximation is satisfactory for plausible values of future carbon concentrations. The shock $\eta_{F,t}$ is a persistent Gaussian shock aimed at capturing the uncertainty pertaining to this relationship. Because this uncertainty is further passed to temperature through (5), $\eta_{F,t}$ eventually drives some randomness into the relationship between atmospheric carbon concentrations and temperatures. In this sense, process $\eta_{F,t}$ captures the uncertainty associated with the so-called climate sensitivity parameter, which characterizes the equilibrium warming response to a doubling of preindustrial CO_2 concentrations (e.g., MacDougall et al., 2017; Barnett et al., 2020).

The atmospheric carbon mass $M_{AT,t}$ appearing in (6) constitutes one of the three reservoirs used here to capture the carbon cycle. The carbon cycle determines the journey of all carbon atoms on earth:[30] a loop between atmosphere, land, and ocean. We denote by M_t the vector whose components are the carbon masses in atmosphere (AT), upper ocean (UP), and lower ocean (LO). The carbon cycle is described as

[27] Consistently with the formulation of the Paris Agreement's objectives, we use the 1850-1900 baseline period as an approximation of the pre-industrial period.

[28] See, e.g., Ramaswamy et al. (2001) for a discussion of the relationship between global temperatures and radiative forcings.

[29] Carbon dioxide is considered as the main greenhouse gas that is due to human activity through the burning of fossil fuels.

[30] The main greenhouse gases containing carbon are also the most active in the atmosphere: carbon dioxide (CO_2) and methane (CH_4).

follows:

$$M_t = \begin{bmatrix} M_{AT,t} \\ M_{UP,t} \\ M_{LO,t} \end{bmatrix} = \varphi^{\Delta t} M_{t-1} + \frac{\Delta t}{3.666} \begin{bmatrix} \mathscr{E}_{t-1} \\ 0 \\ 0 \end{bmatrix}, \tag{7}$$

where φ is a square matrix describing yearly transfers of carbon between atmosphere and oceans. (The column components of φ sum to one.) $\mathscr{E}_{t-1}$ accounts for total carbon dioxide (CO_2) emitted into the atmosphere for each year of period t (one period lasts $\Delta t = 5$ years), converted into carbon masses by applying the conversion rate $1/3.666$. These total emissions $\mathscr{E}_t$ are defined similarly as radiative forcings, with an exogenous and an endogenous components:

$$\mathscr{E}_t = \mathscr{E}_{land,t} + \mathscr{E}_{ind,t} + N_t, \tag{8}$$

where $\mathscr{E}_{ind,t}$ are industrial emissions due to human activity, and $\mathscr{E}_{land,t}$ represents an exogenous component including, in particular, emissions due to deforestation. Industrial emissions, which are assumed to grow as planned capital (K_t^* in Subsection 4.2), are the main constituents of temperature warming. The last component of $\mathscr{E}_t$, namely N_t, is a persistent shock whose probability of occurring increases with temperature in the atmosphere. This variable intends to capture those feedback effects documented in the literature on tipping points (Lenton et al., 2008). Tipping points stem from the existence of feedback loops in our environment; they underlie arrows (b)↔(e) in Figure 1.[31,32] A positive feedback loop amplifies the positive imbalances in radiative forcings by creating a vicious circle strengthening global warming. Examples of positive feedback loop commonly accepted by the scientific community include (a) the release of tons of methane trapped in the permafrost, and (b) the acidification of oceans—the first CO_2 absorbers on Earth, closely followed by the forest ecosystem. If one of these loops is triggered, the probability of triggering the next one jumps, giving rise to tipping point mechanisms (Lemoine and Traeger, 2016; Steffen et al., 2018; Dietz et al., 2020). In our econometric specification, this is captured by drawing N_t from a gamma-zero distribution, which is a distribution featuring a Dirac mass at zero (Monfort et al., 2017), and we make the probability of having a non-zero N_t depend on T_{AT}. In our setting, the probability of having a non-zero N_t is typically small, but if it happens (i.e. when N_t jumps), emissions experiment sudden and large increases, which further increases temperature, and so on.[33]

We augment the model with global mean sea level, which we denote by H_t (with $H_0 = 0.13$, from

[31] Earth is composed of an unknown number of feedback loops, positive or negative. Negative feedback loops decrease the pressure on global warming by absorbing greenhouse gases from the atmosphere.

[32] While our modeling of feedback loops accommodates sudden and large effects, it does not feature an explicit threshold as in, e.g., Lemoine and Traeger (2014, 2016); Bansal et al. (2016); **?**.

[33] This type of mechanism, called self-excitation, is the essence of the Hawkes (1971) process (see Aït-Sahalia et al., 2015, for an application to the modeling of financial contagion).

Vermeer and Rahmstorf (2009)). To do so, we employ the specification proposed by Vermeer and Rahmstorf (2009), namely:

$$H_t = H_{t-1} + \Delta t \times a_{SAT}(T_{AT,t} - T_{0,S}) + b_{SAT}\Delta T_{AT,t} + \sigma_H \eta_{H,t}, \tag{9}$$

where $T_{0,S}$ is the average atmospheric temperature for the period from 1951 to 1980. Equations of the form (9) are called "semi-empirical." The fundamental idea of semi-empirical approaches is to exploit the link between global sea level and global temperature in past observational data for projecting the future.[34]

4.2 Economic block

Let us now discuss the economic block of the model. We consider a standard production economy where capital quality can be damaged by climatic disasters. On each period, agents allocate production (Y_t) between consumption (C_t), investment in productive capital (Inv_t), and investment in low carbon emissions technologies (Ψ_t).

The production of date t is given by:

$$Y_t = A_t K_t, \quad \text{with } A_t = \bar{A} + \sigma_A \eta_{A,t}, \tag{10}$$

where A_t and K_t are productivity, and the quantity of productive capital, respectively. $\bar{A}$ is the average productivity, and $\eta_{A,t} \sim i.i.d.\mathcal{N}(0,1)$ is a productivity shock. The dynamics of productive capital are governed by:

$$K_t^* = (1-dep)K_{t-1} + Inv_t, \tag{11}$$

$$K_t = \exp(-D_t)K_t^*, \tag{12}$$

where dep is the depreciation rate, and where D_t (≥ 0) represents climatic disasters. As in Gomes et al. (2019), and Miller et al. (2020), K_t^* represents planned capital; productive capital K_t is smaller than K_t^* when climatic disaster occur, i.e., when $D_t > 0$. The last three equations imply that production is persistently affected following climatic disasters. As is the case for N_t (see eq. 8), variable D_t is drawn from a gamma-zero distribution (which features a Dirac mass at zero), and the probability that $D_t > 0$ positively depends on the atmospheric temperature (see eq. 28 in Appendix A.2). Therefore, increasing industrial emissions pushes temperatures upwards, which increases the likelihood of disasters, which, in turn, affect production. This adverse mechanism prompts agents to invest in low-carbon technologies. These technologies allow reducing carbon emissions for a given production level. Specifically, investing

[34] See Rahmstorf et al. (2012) for an evaluation of semi-empirical approaches. Studies investigating the relationship between temperatures and sea level include, among others, Rahmstorf (2007), Rahmstorf (2010), Kopp et al. (2016), and Mengel et al. (2018).

in these technologies allow to reduce the emissions stemming from the production of one unit of goods by a factor μ_t, called mitigation rate (with $0 \leq \mu_t \leq 1$). Increasing μ_t is costly. Associated abatement costs (i.e., investment in low-carbon technologies) are given by:

$$\Psi_t = \Lambda_t Y_t, \quad \text{with } \Lambda_t = \mu_t^{\theta_2} BC_t, \tag{13}$$

where BC_t (deterministically) decreases through time, which reflects that technological progress will reduce the backstop price. The term $\mu_t^{\theta_2}$ captures the fact that, on a given date, the marginal cost of mitigation is increasing (with $\theta_2 > 1$).

Hence, agents face the following trade-off: investing in mitigation reduces long-term risks (making disasters less likely) but comes at the cost of lowering immediate consumption. Agents' decision regarding how to allocate output between mitigation (Ψ_t), investment in productive capital (Inv_t), and consumption (C_t) depends on their preferences, which we take of the Epstein-Zin-Weil type (Epstein and Zin, 1989; Weil, 1989).[35]

To get instant results, we simplify the agents' optimization problem. On the initial date ($t = 0$), agents decide on a parametric path for the mitigation rate μ_t. Formally, the parametric path is:

$$\mu_t = \min\left[\exp\left(-\left|\theta_{a,opt}\right| + \left|\theta_{b,opt}\right| \times t\right); 1\right]. \tag{14}$$

The choice of this parametric time function is based on the usual shapes of emission control rates obtained in standard IAM.[36] On the initial date, agents choose $\theta_{a,opt}$ and $\theta_{b,opt}$ to maximize their current utility. They further commit to that parametric path (while dynamically adjusting C_t and Inv_t over time).[37]

4.3 The resulting affine state dynamics

Solving the model essentially amounts to determining the law of motion of consumption. Online Appendix I.1 shows that, under the prior assumptions, consumption growth is of the form:

$$\Delta c_t = \mu_{c,t} + \sigma_{c,t}\eta_{A,t} - D_t, \tag{15}$$

[35] These preferences allow to dissociate risk aversion and the elasticity of intertemporal substitution (EIS). The latter is taken equal to one (see Appendix A.3 for computational details). Epstein-Zin-Weil preferences, or, more generally, recursive preferences, are widely used to capture equity and bond risk premiums (Bansal and Yaron, 2004). These preferences have been used in numerous recent IAMs (Cai and Lontzek, 2019; Jensen and Traeger, 2014; Lemoine and Traeger, 2014).

[36] See, e.g., Cai and Lontzek (2019), Figure 2.C. Our resulting path is given in Appendix IV.2, where it is compared to the path underlying the 2017 version of the DICE model (Nordhaus, 2017).

[37] In practice, knowing all other model parameters, we numerically look for the values of $\theta_{a,opt}$ and $\theta_{b,opt}$ leading to the highest utility in the current date. (For a given parameterization, the solution to the utility function is given by Prop. 8.) This numerical optimization has to be performed for each considered set of parameters in the context of the calibration approach (see Subsection 4.4); but it is extremely fast.

where $\mu_{c,t}$ and $\sigma_{c,t}$ are simple deterministic functions of the model parameters (see eq. 26 in Appendix A.2). What is key for the tractability of the framework is that the resulting law of motion of the state vector X_t—which gathers all economic and climatic variables introduced above—is of the affine class. Formally, the conditional Laplace transform of X_t, which characterizes the state vector's dynamics, is of the form:

$$\mathbb{E}_t[\exp(u'X_{t+1})] = \exp(\alpha_t(u) + \beta_t(u)'X_t), \tag{16}$$

where functions α_t and β_t deterministically depend on the model parameters (see Proposition 2).[38] Once these functions are known, one can easily deduce the multi-horizon Laplace transform:

$$\mathbb{E}_t[\exp(u'X_{t+h})] = \exp(a_{t,h}(u) + b_{t,h}(u)'X_t), \tag{17}$$

where functions $a_{t,h}$ and $b_{t,h}$ are recursively defined (Corollary 1).

Knowing the multi-horizon Laplace transform (17) is equivalent to knowing the distribution of X_{t+h} conditional on X_t. This implies in particular that, in the present framework, simple inverse Fourier transform can be employed to recover the conditional distribution of any of the state variable, or any linear combination of the variables, at any horizon. To our knowledge, this article is the first to propose formulas for evaluating conditional distributions of macroeconomic and climate variables in an IAM framework. It should be noted that these formulas make it possible to detect immediately whether a given parameterization of the model is consistent or not with a stable economy. (This is more complicated, if not impossible, in models whose solution is based on simulations.)

In terms of pricing, tractability results from (a) the affine property of X_t (eq. 16) together with (b) the fact that the underlying stochastic discount factor $\mathscr{M}_{t,t+1}$ (see Section 3) is exponential affine in X_t.[39] These two ingredients ensure the existence of recursive formulas to price various long-term assets. With respect to standard affine term-structure models,[40] a specificity of the present framework is that functions α_t and β_t depend on time. Online Appendix III shows how to accommodate this time dependency.

4.4 Calibration

Numerous parameters of the model are directly taken from existing literature (see Table 4). However, some of our parameters have not direct equivalent in previous studies; this is notably the case of the parameters governing economic damages (D_t) and positive feedback loops (N_t). In order to address this issue, we employ an original approach that takes advantage of the model tractability. Specifically, a subset of the model parameters is determined by minimizing a criterion that reflects the distance between moments

[38] The Analytic Climate Economy (ACE) model of Traeger (2021) also features an affine state vector. In the ACE model, function β_t does not depend on time, which relates from the fact that this framework does not consider mitigation opportunities.

[39] The fact that the s.d.f. is exponential affine is demonstrated in Proposition 9 of Online Appendix III.1.

[40] See, e.g. Duffie (1996), Duffie et al. (2003), or Piazzesi (2010) for presentations of affine term-structure modeling.

found in the literature and their model-implied equivalents. Let us stress that this calibration approach is infeasible in the context of standard IAMs, whose resolution is not immediate, or for which simulations are necessary to compute long-term expectations or variances (such as the expectation or variance of temperatures in 2100, say). By contrast, such moments are here available in closed-form (see Online Appendix II).

Appendix B contains details regarding the calibration approach. Let us however briefly mention the targeted moments: (a) the regression slope of cumulated climate-related damages on atmospheric temperatures in 2100 (target based on Burke et al., 2015b, Figure 5.d); (b) the expected global atmospheric temperature in 2100 (target based on IPCC's Representative Concentration Pathways, RCPs);[41] (c) the standard deviation of global atmospheric temperature in 2100 (target based on RCPs); (d) the expected contribution of feedback loops on the 2100 global temperature (target based on Burke et al., 2012); (e) the expected cumulated emissions in 2100 (target based on Burke et al., 2012); (f) the 80-year real risk-free yield (target based on very-long-term rates computed by the U.S. Department of the Treasury); (g) the expected sea level in 2100 (target based on RCPs); (h) the standard deviation of sea level in 2100 (target based on Mengel et al., 2016, Figure 4). Table 2 of Appendix B shows the parameters resulting from this moment-fitting approach.

Because the social cost of carbon (SCC) occupies a central place in the IAM literature, it is interesting to evaluate it in our calibrated framework. Our SCC estimate is $167 per ton of carbon, which is higher than the values obtained in most alternative studies (see Appendix C). This high value may result from the fact that our model is one of the very few that tries and capture climate-change feedback loops.

5 Results

5.1 Temperature-indexed swaps and bonds

This subsection presents model-implied prices of temperature-indexed swaps and bonds (presented in Section 3). We also discuss the climate risk premiums, defined as those components of climate linkers' prices that would be null under the "expectation hypothesis", i.e. in a world where agents would not be risk averse.[42]

Let us start with temperature-indexed swaps (TIS, see Definition 1). Panel (a) of Figure 2 shows the term-structure of temperature-indexed swaps, in orange. More specifically, it shows TIS rates ($T^S_{t,h}$) for different maturities h. The blue line displays expected atmospheric temperatures, i.e., $\mathbb{E}_t(T_{AT,t+h})$. If agents were not risk-averse, then TIS rates would coincide with expected temperatures (see eq. (1)). In other words, the deviation between the blue and the orange lines reflects climate risk premiums. The

[41] RCP scenarios are based on Clarke et al. (2007); Smith and Wigley (2006); Wise et al. (2009); Fujino et al. (2006); Hijioka et al. (2008). Specifically, we use RCP45 and RCP60 scenarios.

[42] More precisely, these counterfactual prices would be the one prevailing under the "local expectation hypothesis", as convexity adjustments would be taken into account (see Piazzesi, 2010, Section 2.2).

results indicate for instance that the TIS rate—which can be seen as a risk-adjusted expected temperature, as explained below eq. (2)—lies about 0.25°C above expected temperatures for 2100.

[Insert Figure 2 about here]

Panel (b) of Figure 2 shows the term structure of Temperature-Indexed Bond rates. Note that these yields are real rates, as the model does not account for inflation. We consider different values of χ, which determines the sensitivity of the payoff to realized atmospheric temperatures (see Definition 2). The figure also displays zero-coupon bond yields, in black. As explain in Definition 2, the expected payoffs of a TIB is equal to one if the reference temperature ($T^0_{t,h}$) is set to the expected temperature. Hence, a TIB and a (standard) zero-coupon bond have the same expected payoff. However, Panel (b) of Figure 2 shows that the equilibrium prices of TIBs are higher than those of standard bonds (since yields-to-maturity are lower). This results from the fact that a TIB also provides insurance against temperature risks. Because of these hedging properties, investors are willing to buy TIBs even if they provide lower expected returns. That is, the difference between the black and orange lines are risk premiums. Naturally, the higher χ, the higher the premium. Focussing on $\chi = 1$, we obtain that the yield-to-maturity of a TIB maturing in 2100 is about 25 basis points lower than the zero-coupon bond providing the same expected payoff.

The fact that TIBs' yields-to-maturity depend on the payoff's sensitivity to realized atmospheric temperatures (χ) illustrates the fact that appropriate discount rates depend on the climate-risk exposure of the considered asset. This relates to the debate on the social discount rate to be used to assess climate-related public policy actions (see, e.g., Gollier, 2013; Arrow et al., 2014; Gollier and Hammitt, 2014; Bauer and Rudebusch, 2020): similar mechanisms indeed explain why one has to adapt the discount rate to the risk profile of the flow of net benefits generated by the policy under scrutiny. As discussed in Dietz et al. (2018), if a policy tends to raise the collective risk borne by a community of risk-averse agents, this policy should be penalized by increasing the discount rate by a risk premium specific to the policy—and vice versa if the policy tends to hedge collective risk.

[Insert Figure 3 about here]

Figure 3 illustrates the sensitivity of swap-embedded climate risk premiums to the magnitude of disasters (μ_D) and of the feedback loops (μ_N). These two parameters are crucial to characterize climate-related risks. In Panel (a), we show how expected temperatures and TIS rates—that can be interpreted as risk-adjusted expected temperatures—are affected by changes in these two parameters. It appears in particular that expected temperatures only weakly depend on the magnitude of economic disasters. On the contrary, TIS rates (i.e. risk-adjusted temperatures) strongly depend on both parameters. As explained above, the difference between TIS rates and expected temperatures is a climate risk premium. Panel (b) of Figure 3 displays the contribution of these premiums in the TIS rate. It appears that risk premiums increase w.r.t. to both parameters.

[Insert Figure 4 about here]

Figure 4 provides another illustration of the sensitivity of risk premiums to the magnitude of disasters. More precisely, Panel (a) shows how TIS-embedded risk premiums vary with μ_D for three different values of the feedback loop magnitude (μ_N): the first is zero, the second is its calibrated value ($\mu_N \approx 30$), and the third is larger ($\mu_N = 40$). Three remarks are in order. First, the risk premium is highly nonlinear in the magnitude of disasters. Second, for very low values of μ_D, the risk premium is negative. In this case, high temperatures are not worrying because they do not give rise to disasters. On the contrary, high temperatures then reflect periods of higher-than-expected growth—with no risk attached. Therefore, for such specification (i.e., $\mu_D \approx 0$), agents perceive high-temperature states as "good states". Accordingly, financial instruments that pay relatively more in these states, such as TIS, embed negative risk premiums. Let us stress that this situation, which prevails only for very small values of μ_D, is far from our baseline specification. In the latter, μ_D is substantial, and high temperatures have disastrous implications. Third, for each value of μ_N, there exists a value of μ_D for which risk premiums explode, resulting in a vertical asymptote. (The higher μ_N, the lower this maximal value of μ_D.) Hence, when disasters are expected to be large, insuring against climate change can become infinitely costly in our model, a situation that echoes that studied by Weitzman (2009, 2014). Panels (b) and (c) of Figure 4 show that these limit parameterizations also correspond to infinite model-implied social costs of carbon (SCCs), and infinitely-negative long-term interest rates, respectively.

5.2 Temperature options

In the present section, we discuss the pricing of options, whose payoffs nonlinearly depend on temperatures (see Definition 3), contrary to TISs and TIBs. Our framework offers quasi-closed-form valuation formulas for these options.[43] These formulas rely on Fourier analysis, that allows to recover probability density functions (p.d.f.) of any linear combination of the state variables, at any horizon. This is illustrated by Figure 5, whose Panels (a) and (b) respectively represent the physical and risk-adjusted (i.e., including risk premiums) p.d.f. of atmospheric temperatures, up to 2100.[44] Taken together, the plots show that the risk-adjusted p.d.f. is shifted up w.r.t. the physical one. That is, when it comes to price temperature-indexed instruments, risk-adjusted probabilities overweight those states of the world where temperature is higher. This is because the model recognizes that high temperatures characterize states of high marginal utility (lower consumption), which tends to increase the associate risk-adjusted (or Arrow-Debreu) probabilities. Panel (c) of Figure 5 plots the model-implied physical and risk-adjusted p.d.f. of atmospheric temperatures in 2100. Consistently with what precedes, we see that the risk-adjusted p.d.f. is shifted to the right w.r.t. the

[43] Solutions are quasi-explicit as they involve numerical computations of integrals. Importantly, these integrals are one-dimensional, whatever the number of state variables considered in the model. See Proposition 11 of the online appendix for more details; this proposition builds on Duffie et al. (2000).

[44] See discussion below eq. (2), and Footnote 25, for details onrisk-adjusted probabilities.

physical one. Moreover, it appears that the risk-adjusted p.d.f. is flatter than the physical one, indicating that the overall quantity of risk is higher in the risk-adjusted world.

[Insert Figure 5 about here]

Let us show how this translates into option prices. For expository purposes, we will focus on digital options, whose prices can be interpreted as risk-adjusted probabilities that future temperatures will exceed a certain threshold—namely, the option's strike (T_K in Definition 3). Figure 6 plots the prices of such digital options for T_K =2.5, 3 and 4, and maturities up to 2100. More precisely, we report option prices divided by the prices of zero-coupon of matching maturities; this makes these prices comparable to probabilities, and we call them risk-adjusted probabilities. (See Footnote 25 for a detailed definition of risk-adjusted probabilities.) Consistently with what precedes, we observe that risk-adjusted probabilities are substantially higher than their physical counterparts. We also find that ratios between risk-adjusted and physical probabilities increase with the temperature strike. The ratio can be substantial for high temperature. For $T_K = 3°$C and, focussing on the 2100 maturity, the risk-adjusted probabilities are about 10% larger than the model-implied physical probability of exceeding this threshold. That type of result is reminiscent of a finding of the disaster-risk pricing literature: risk premiums can represent the bulk of the prices of those financial instruments providing larger payoffs in disastrous situations (financial meltdowns, defaults of large corporate or sovereign entities, e.g., Elton et al., 2001; Coval et al., 2009; Monfort et al., 2021; Gouriéroux et al., 2021).

[Insert Figure 6 about here]

5.3 Alternative indexation variables

While temperature stands as an indexation variable of interest, other variables can be considered. Definitions 1, 2, and 3 could be easily adjusted to introduce, respectively, swaps, bonds, and options with payoffs depending on these alternative climate-related variables. In this subsection, we focus on two of them, namely the atmospheric carbon concentration, and the sea level.[45]

Figure 7 displays the physical and risk-adjusted distributions of future carbon concentrations. As for temperatures, the risk-adjusted distribution of carbon concentrations is more disperse and shifted to the right compared to its physical counterpart (see Panel (c) of Figure 7). This would translate, in particular, in the existence of positive risk premiums in carbon-concentration swaps; these risk premiums correspond to the difference between the orange and blue lines in Panel (b).

[Insert Figure 7 about here]

[45] Derivatives indexed on sea levels are discussed in Bloch et al. (2010, 2011).

Let us now turn to sea levels. As shown by Figure 8, the model predicts an increase in the mean sea level of about 0.45 meter by 2100. The corresponding risk-adjusted increase is of 0.47 meter. That is, if sea level swaps were to be traded, (unadjusted) market quotes would overestimate physical expectations of sea level rises.

[Insert Figure 8 about here]

6 Concluding remarks

This paper makes a case for climate linkers. We define climate linkers as long-dated financial instruments (bonds, swaps, and options) with payoffs indexed to climate-related variables, e.g., temperatures, carbon concentrations, or sea levels.

Naturally, even if a liquid market for climate-indexed instruments was to emerge, it could not eliminate the fundamental risk that society faces, as associated net exposures eventually cancel out. Some entities will have to bear the risks. We, however, argue that such instruments may contribute to the sharing of long-term climate risks. Another key benefit would be informational, as the prices of such instruments would reveal real-time market expectations regarding future climate. This information would, for instance, be useful to appraise how investors assess the credibility of measures aimed at fighting climate risks, or how they view the influence of economic or political news on climate. Furthermore, these measures would be available in real-time, and at high frequency.

On the methodological front, we develop a tractable integrated assessment model (IAM). This model can be solved instantaneously and offers quasi-analytical pricing formulas for climate-indexed bonds, swaps, or options. Tractability results from the fact that the state vector is affine conditional on a few deterministic processes (such as, e.g., the backstop price, as in the DICE model of Nordhaus, 2017). Importantly, the affine property of the state vector does not preclude disasters; in particular: (i) the model allows for sudden climate-related falls in consumption, and (ii) the model captures adverse feedback loops reflecting, e.g., potential permafrost-related carbon releases.

We exploit the model tractability at the calibration stage. While we take many parameters directly from the literature, we determine several others—typically those that have no direct equivalent in previous studies—by minimizing a criterion capturing the distance between model-implied and targeted moments. For instance, we look for a model parametrization that is consistent with available estimations of the temperature effects of permafrost releases.

Equipped with our model, we examine, in particular, climate risk premiums. Because of the insurance provided by a bond (positively) indexed on temperature, investors would demand a lower average return on such a bond than on conventional bonds. Our findings highlight the sensitivity of climate risk premiums to the assumptions regarding (i) damages associated with temperature increases and (ii) feedback effects between temperatures and emissions.

References

Aït-Sahalia, Y., Cacho-Diaz, J., and Laeven, R. J. (2015). Modeling Financial Contagion Using Mutually Exciting Jump Processes. *Journal of Financial Economics*, 117(3):585–606.

Andersson, M., Bolton, P., and Samama, F. (2019). Hedging Climate Risk. *Financial Analysts Journal*, 72:13–32.

Arrow, K. J., Cropper, M. L., Gollier, C., Groom, B., Heal, G. M., Newell, R. G., Nordhaus, W. D., Pindyck, R. S., Pizer, W. A., Portney, P. R., and Ste, T. (2014). Should Governments Use a Declining Discount Rate in Project Analysis? *Review of Environmental Economics and Policy*, 8(2):145–163.

Baker, M., Bergstresser, D., Serafeim, G., and Wurgler, J. (2018). Financing the Response to Climate Change: The Pricing and Ownership of U.S. Green Bonds. NBER Working Papers 25194, National Bureau of Economic Research, Inc.

Bansal, R., Kiku, D., and Ochoa, M. (2019). Climate Change Risk. Technical report.

Bansal, R., Ochoa, M., and Kiku, D. (2016). Climate Change and Growth Risks. Working Paper 23009, National Bureau of Economic Research.

Bansal, R. and Yaron, A. (2004). Risks for the Long Run: A Potential Resolution of Asset Pricing Puzzles. *Journal of Finance*, 59:1481–1509.

Barnett, M., Brock, W., Hansen, L. P., and Hong, H. (2020). Pricing Uncertainty Induced by Climate Change. *Review of Financial Studies*, 33(3):1024–1066.

Batten, S., Sowerbutts, R., and Tanaka, M. (2016). Let's Talk About the Weather: The Impact of Climate Change on Central Banks. Bank of England working papers 603, Bank of England.

Battiston, S., M. A. M. I. et al. (2017). A Climate Stress-Test of the Financial System. *Nature Climate Change*, 7:283–288.

Bauer, M. D. and Rudebusch, G. D. (2020). The Rising Cost of Climate Change: Evidence from the Bond Market. Working Paper Series 2020-25, Federal Reserve Bank of San Francisco.

Berliner, B. (1985). Large Risks and Limits of Insurability. *The Geneva Papers on Risk and Insurance*, 10(37):313–329.

Bloch, D., Annan, J., and Bowles, J. (2010). Cracking the Climate Change Conundrum with Derivatives. *Wilmott Journal*, 2(5):271–287.

Bloch, D., Annan, J., and Bowles, J. (2011). Applying Climate Derivatives to Flood Risk Management. *Wilmott*, 2011(56):88–103.

Bolton, P., Després, M., da Silva, L. A. P., Samama, F., and Svartzman, R. (2020). *The Green Swan*. Number 31 in BIS Books. Bank for International Settlements.

Brace, A., Gątarek, D., and Musiela, M. (1997). The Market Model of Interest Rate Dynamics. *Mathematical Finance*, 7(2):127–155.

Braun, A. (2016). Pricing in the Primary Market for Cat Bonds: New Empirical Evidence. *Journal of Risk and Insurance*, 83(4):811–847.

Brockett, P. L., Wang, M., and Yang, C. (2005). Weather Derivatives and Weather Risk Management. *Risk Management and Insurance Review*, 8(1):127–140.

Bruggeman, V., Faure, M. G., and Fiore, K. (2010). The Government as Reinsurer of Catastrophe Risks? *The Geneva Papers on Risk and Insurance - Issues and Practice*, 35(3):369–390.

Burke, E. J., Hartley, I. P., and Jones, C. D. (2012). Uncertainties in the Global Temperature Change Caused by Carbon Release from Permafrost Thawing. *The Cryosphere*, 6(5):1063–1076.

Burke, M., Dykema, J., Lobell, D. B., Miguel, E., and Satyanath, S. (2015a). Incorporating Climate Uncertainty into Estimates of Climate Change Impacts. *The Review of Economics and Statistics*, 97(2):461–471.

Burke, M., Hsiang, S. M., and Miguel, E. (2015b). Global Non-Linear Effect of Temperature on Economic Production. *Nature*, 527(7577):235–239.

Cai, Y. and Judd, K. L. (2014). Advances in Numerical Dynamic Programming and New Applications. In Schmedders, K. and Judd, K. L., editors, *Handbook of Computational Economics Vol. 3*, volume 3 of *Handbook of Computational Economics*, chapter 8, pages 479 – 516. Elsevier.

Cai, Y. and Lontzek, T. S. (2019). The Social Cost of Carbon with Economic and Climate Risks. *Journal of Political Economy*, 127(6):2684–2734.

Campbell, J. Y. and Shiller, R. J. (1996). A Scorecard for Indexed Government Debt. In *NBER Macroeconomics Annual 1996, Volume 11*, NBER Chapters, pages 155–208. National Bureau of Economic Research, Inc.

Campbell, S. D. and Diebold, F. X. (2005). Weather Forecasting for Weather Derivatives. *Journal of the American Statistical Association*, 100:6–16.

Cao, M. and Wei, J. (2004). Weather Derivatives Valuation and Market Price of Weather Risk. *Journal of Futures Markets*, 24(11):1065–1089.

Cevik, S. and Jalles, J. T. (2020). This Changes Everything: Climate Shocks and Sovereign Bonds. IMF Working Papers 2020/079, International Monetary Fund.

Charpentier, A. (2008). Insurability of Climate Risks. *The Geneva Papers on Risk and Insurance - Issues and Practice*, 33(1):91–109.

Charpentier, A. and Le Maux, B. (2014). Natural Catastrophe Insurance: How Should the Government Intervene? *Journal of Public Economics*, 115(C):1–17.

Clarke, L., Edmonds, J., Jacoby, H., Pitche, H., Reilly, J., and Richels, R. (2007). Scenarios of Greenhouse Gas Emissions and Atmospheric Concentrations. Sub-report 2.1A of Synthesis and Assessment Product 2.1 by the U.S. Climate Change Science Program and the Subcommittee on Global Change Research. Department of Energy, Office of Biological & Environmental Research, Washington, 7 DC., USA, 154 pp.

Cochrane, J. H. and Piazzesi, M. (2005). Bond Risk Premia. *American Economic Review*, 95(1):138–160.

Coval, J. D., Jurek, J. W., and Stafford, E. (2009). Economic Catastrophe Bonds. *American Economic Review*, 99(3):628–666.

Cummins, J. D. and Weiss, M. A. (2009). Convergence of Insurance and Financial Markets: Hybrid and Securitized Risk-Transfer Solutions. *Journal of Risk & Insurance*, 76(3):493–545.

D'Amico, S., Kim, D. H., and Wei, M. (2018). Tips from TIPS: The Informational Content of Treasury Inflation-Protected Security Prices. *Journal of Financial and Quantitative Analysis*, 53(1):395–436.

Daniel, K. D., Litterman, R. B., and Wagner, G. (2019). Declining CO_2 Price Paths. *Proceedings of the National Academy of Sciences*, 116(42):20886–20891.

Davies, R., Haldane, A. G., Nielsen, M., and Pezzini, S. (2014). Measuring the Costs of Short-Termism. *Journal of Financial Stability*, 12:16–25. Reforming finance.

Desmet, K., Kopp, R. E., Kulp, S. A., Nagy, D. K., Oppenheimer, M., Rossi-Hansberg, E., and Strauss, B. H. (2021). Evaluating the Economic Cost of Coastal Flooding. *American Economic Journal: Macroeconomics*, 13(2):444–486.

Dietz, S., Bowen, A., Dixon, C., and Gradwell, P. (2016). Climate Value at Risk of Global Financial Assets. *Nature Climate Change*, 6:676–680.

Dietz, S., Gollier, C., and Kessler, L. (2018). The Climate Beta. *Journal of Environmental Economics and Management*, 87(C):258–274.

Dietz, S., van der Ploeg, R., Rezai, A., and Venmans, F. (2020). Are Economists Getting Climate Dynamics Right and Does It Matter? Technical report.

Duffie, D. (1996). *Dynamic Asset Pricing Theory*. Princeton University Press, Princeton, New Jersey, second edition.

Duffie, D., Filipovic, D., and Schachermayer, W. (2003). Affine Processes and Applications in Finance. *Annals of Applied Probability*, 13(3):984–1053.

Duffie, D., Pan, J., and Singleton, K. (2000). Transform Analysis and Asset Pricing for Affine Jump-Diffusions. *Econometrica*, 68(6):1343–1376.

Elton, E. J., Gruber, M. J., Agrawal, D., and Mann, C. (2001). Explaining the Rate Spread on Corporate Bonds. *Journal of Finance*, 56(1):247–277.

Engle, R. F., Giglio, S., Kelly, B., Lee, H., Stroebel, J., and Karolyi, A. (2020). Hedging Climate Change News. *Review of Financial Studies*, 33(3):1184–1216.

Epstein, L. G. and Zin, S. E. (1989). Substitution, Risk Aversion, and the Temporal Behavior of Consumption and Asset Returns: A Theoretical Framework. *Econometrica*, 57(4):937–69.

Folini, D., Kubler, F., Malova, A., and Scheidegger, S. (2021). The Climate in Climate Economics. Ssrn working papers.

Fujino, J., Kainuma, R. N. M., Masui, T., and Matsuoka, Y. (2006). Multi-gas mitigation analysis on stabilization scenarios using AIM global model. Multigas Mitigation and Climate Policy. *The Energy Journal Special Issue*.

García, J. A. and Van Rixtel, A. (2007). Inflation-Linked Bonds from a Central Bank Perspective. Occasional Paper Series 62, European Central Bank.

Giglio, S., Kelly, B. T., and Stroebel, J. (2020). Climate Finance. NBER Working Papers 28226, National Bureau of Economic Research, Inc.

Giovannini, A. and Weil, P. (1989). Risk Aversion and Intertemporal Substitution in the Capital Asset Pricing Model. NBER Working Papers 2824, National Bureau of Economic Research, Inc.

Gollier, C. (2013). *Pricing the Planet's Future: The Economics of Discounting in an Uncertain World*. Princeton University Press.

Gollier, C. and Hammitt, J. K. (2014). The Long-Run Discount Rate Controversy. *Annual Review of Resource Economics*, 6(1):273–295.

Gomes, J. F., Grotteria, M., and Wachter, J. A. (2019). Cyclical Dispersion in Expected Defaults. *Review of Financial Studies*, 32(4):1275–1308.

Gouriéroux, C., Monfort, A., Mouabbi, S., and Renne, J.-P. (2021). Disastrous Defaults. *Review of Finance*, forthcoming.

Grishchenko, O., Vanden, J. M., and Zhang, J. (2016). The Informational Content of the Embedded Deflation Option in TIPS. *Journal of Banking & Finance*, 65(C):1–26.

Gürtler, M., Hibbeln, M., and Winkelvos, C. (2016). The Impact of the Financial Crisis and Natural Catastrophes on CAT Bonds. *Journal of Risk & Insurance*, 83(3):579–612.

Hambel, C., Kraft, H., and Schwartz, E. (2021). Optimal Carbon Abatement in a Stochastic Equilibrium Model with Climate Change. *European Economic Review*, 132(C).

Hansen, L. P. and Jagannathan, R. (1991). Implications of Security Market Data for Models of Dynamic Economies. *Journal of Political Economy*, 99(2):225–262.

Hansen, L. P. and Richard, S. F. (1987). The Role of Conditioning Information in Deducing Testable. *Econometrica*, 55(3):587–613.

Hauer, M., Evans, J., and Mishra, D. (2016). Millions Projected to Be at Risk from Sea-level Rise in the Continental United States. *Nature Climate Change*, 6:691–695.

Hawkes, A. G. (1971). Spectra of Some Self-Exciting and Mutually Exciting Point Processes. *Biometrika*, 58(1):83–90.

Hijioka, Y., Matsuoka, Y., Nishimoto, H., Masui, M., and Kainuma, M. (2008). Global GHG emissions scenarios under GHG concentration stabilization targets. *Journal of Global Environmental Engineering*, (13):97–108.

Hong, H., Karolyi, G. A., and Scheinkman, J. A. (2020). Climate Finance. *Review of Financial Studies*, 33(3):1011–1023.

Huynh, T. D. and Xia, Y. (2020). Climate Change News Risk and Corporate Bond Returns. *Journal of Financial and Quantitative Analysis*, pages 1–25.

International Monetary Fund (2019). Sustainable Finance: Looking Farther. Global Financial Stability Report, Chapter 6 October 2019, IMF.

IPCC (2014). *IPCC, 2014: Climate Change 2014: Synthesis Report. Contribution of Working Groups I, II and III to the Fifth Assessment Report of the Intergovernmental Panel on Climate Change*. Core Writing Team, R.K. Pachauri and L.A. Meyer (eds.), IPCC, Geneva, Switzerland.

Jamshidian, F. (1989). An Exact Bond Option Formula. *The Journal of Finance*, 44(1):205–209.

Jensen, S. and Traeger, C. P. (2014). Optimal Climate Change Mitigation under Long-Term Growth Uncertainty: Stochastic Integrated Assessment and Analytic Findings. *European Economic Review*, 69:104–125.

Karydas, C. and Xepapadeas, A. (2019). Pricing Climate Change Risks: CAPM with Rare Disasters and Stochastic Probabilities. CER-ETH Economics working paper series 19/311, CER-ETH - Center of Economic Research (CER-ETH) at ETH Zurich.

Kopp, R. E., Kemp, A. C., Bittermann, K., Horton, B. P., Donnelly, J. P., et al. (2016). Temperature-Driven Global Sea-Level Variability in the Common Era. *Proceedings of the National Academy of Sciences*, 113(11):E1434–E1441.

Krueger, P., Sautner, Z., and Starks, L. T. (2021). The Importance of Climate Risks for Institutional Investors. *Review of Financial Studies*, forthcoming.

Lannoo, K. and Thomadakis, A. (2020). Derivatives in Sustainable Finance, Enabling the Green Transition. CEPS- ECMI Study, Centre for European Policy Studies.

Larcker, D. F. and Watts, E. M. (2020). Where's the Greenium? *Journal of Accounting and Economics*, 69(2).

Lemoine, D. (2021). The Climate Risk Premium: How Uncertainty Affects the Social Cost of Carbon. *Journal of the Association of Environmental and Resource Economists*, 8(1):27–57.

Lemoine, D. and Traeger, C. (2014). Watch your step: Optimal policy in a tipping climate. *American Economic Journal: Economic Policy*, 6(1):137–66.

Lemoine, D. and Traeger, C. (2016). Economics of Tipping the Climate Dominoes. *Nature Climate Change*, 6:514–519.

Lenton, T. M., Held, H., Kriegler, E., Hall, J. W., Lucht, W., Rahmstorf, S., and Schellnhuber, H. J. (2008). Tipping Elements in the Earth's Climate System. *Proceedings of the National Academy of Sciences*, 105(6):1786–1793.

MacDougall, A. H., Swart, N. C., and Knutti, R. (2017). The Uncertainty in the Transient Climate Response to Cumulative CO2 Emissions Arising from the Uncertainty in Physical Climate Parameters. *Journal of Climate*, 30:813–827.

Mengel, M., Levermann, A., Frieler, K., Robinson, A., Marzeion, B., and Winkelmann, R. (2016). Future Sea Level Rise constrained by Observations and Long-Term Commitment. *Proceedings of the National Academy of Sciences*, 113(10):2597–2602.

Mengel, M., Nauels, A., Rogelj, J., et al. (2018). Committed Sea-Level Rise Under the Paris Agreement and the Legacy of Delayed Mitigation Action. *Nature Communication*, 9:1–10.

Miller, M., Paron, J. D., and Wachter, J. A. (2020). Sovereign Default and the Decline in Interest Rates. Technical report.

Mills, E. (2005). Insurance in a Climate of Change. *Science*, 309(5737):1040–1044.

Miltersen, K. R., Sandmann, K., and Sondermann, D. (1997). Closed Form Solutions for Term Structure Derivatives with Log-Normal Interest Rates. *Journal of Finance*, 52(1):409–430.

Monasterolo, I. (2020). Climate Change and the Financial System. *Annual Review of Resource Economics*, 12:299–320.

Monfort, A., Pegoraro, F., Renne, J.-P., and Roussellet, G. (2017). Staying at Zero with Affine Processes: An Application to Term Structure Modelling. *Journal of Econometrics*, 201(2):348–366.

Monfort, A., Pegoraro, F., Renne, J.-P., and Roussellet, G. (2021). Affine Modeling of Credit Risk, Pricing of Credit Events,

and Contagion. *Management Science*, forthcoming.
Nordhaus, W. D. (1992). An Optimal Transition Path for Slowing Climate Change. *Science*, 20:1315–1319.
Nordhaus, W. D. (2017). Revisiting the Social Cost of Carbon. *Proceedings of the National Academy of Sciences*, 114(7):1518–1523.
Painter, M. (2020). An Inconvenient Cost: The Effects of Climate Change on Municipal Bonds. *Journal of Financial Economics*, 135(2):468–482.
Pérez-González, F. and Yun, H. (2013). Risk Management and Firm Value: Evidence from Weather Derivatives. *Journal of Finance*, 68(5):2143–2176.
Piazzesi, M. (2010). Affine Term Structure Models. In *Handbook of Financial Econometrics, Volume 1*, chapter 12, pages 389–472. Yacine Aït-Sahalia and Lars Peter Hansen North Holland edition.
Piazzesi, M. and Schneider, M. (2007). Equilibrium Yield Curves. In *NBER Macroeconomics Annual 2006, Volume 21*, NBER Chapters, pages 389–472. National Bureau of Economic Research, Inc.
Price, R. T. (1997). The Rationale and Design of Inflation-Indexed Bonds. IMF Working Papers 1997/012, International Monetary Fund.
Purnanandam, A. and Weagley, D. (2016). Can Markets Discipline Government Agencies? Evidence from the Weather Derivatives Market. *Journal of Finance*, 71(1):303–334.
Rahmstorf, S. (2007). A Semi-Empirical Approach to Projecting Future Sea-Level Rise. *Science*, 315(5810):368–370.
Rahmstorf, S. (2010). A New View on Sea Level Rise. *Nature Climate Change*, 1:44–45.
Rahmstorf, S., Perrette, M., and Vermeer, M. (2012). Testing the Robustness of Semi-Empirical Sea Level Projections. *Climate Dynamics*, 39:861–875.
Ramaswamy, V., Boucher, O., Haigh, J., Hauglustaine, D., Haywood, J., et al. (2001). *Radiative Forcing of Climate Change*.
Schaefer, K., Lantuit, H., Romanovsky, V. E., Schuur, E. A. G., and Witt, R. (2014). The Impact of the Permafrost Carbon Feedback on Global Climate. *Environmental Research Letters*, 9(8):1–9.
Schorfheide, F., Song, D., and Yaron, A. (2018). Identifying Long-Run Risks: A Bayesian Mixed-Frequency Approach. *Econometrica*, 86(2):617–654.
Slawinski, N., Pinkse, J., Busch, T., and Banerjee, S. B. (2017). The Role of Short-Termism and Uncertainty Avoidance in Organizational Inaction on Climate Change: A Multi-Level Framework. *Business & Society*, 56(2):253–282.
Smith, S. and Wigley, T. (2006). Multi-Gas Forcing Stabilization with the MiniCAM. *Energy Journal*, (Special Issue 3):373–391.
Standard & Poor's Global (2017). How Environmental and Climate Risks and Opportunities Factor Into Global Corporate Ratings – An Update. S&P Global - Ratings November 2017, Standard & Poor's.
Steffen, W., Rockström, J., Richardson, K., Lenton, T. M., Folke, C., et al. (2018). Trajectories of the Earth System in the Anthropocene. *Proceedings of the National Academy of Sciences*, 115(33):8252–8259.
Stern, N. (2007). *The Economics of Climate Change: The Stern Review*. Cambridge University Press.
Swiss Re Institute (2020). Natural Catastrophes in Times of Economic Accumulation and Climate Change. Technical report, Swiss Re.
Traeger, C. (2021). ACE - Analytic Climate Economy. CEPR Discussion Papers 15968, C.E.P.R. Discussion Papers.
van den Bremer, T. S. and van der Ploeg, F. (2021). The Risk-Adjusted Carbon Price. *American Economic Review*, 111(9):2782–2810.
Vermeer, M. and Rahmstorf, S. (2009). Global Sea Level Linked to Global Temperature. *Proceedings of the National Academy of Sciences*, 106(51):21527–21532.
Weil, P. (1989). The Equity Premium Puzzle and the Risk-Free Rate Puzzle. *Journal of Monetary Economics*, 24(3):401–421.
Weitzman, M. L. (2009). On Modeling and Interpreting the Economics of Catastrophic Climate Change. *The Review of Economics and Statistics*, 91(1):1–19.
Weitzman, M. L. (2013). Tail-Hedge Discounting and the Social Cost of Carbon. *Journal of Economic Literature*, 51(3):873–882.
Weitzman, M. L. (2014). Fat Tails and the Social Cost of Carbon. *American Economic Review: Papers & Proceedings*, 104(5):544–546.
Wise, M., Calvin, K., Thomson, A., Clarke, L., Bond-Lamberty, B., Sands, R., Smith, S., Janetos, A., and Edmonds, J. (2009). Implications of Limiting CO2 Concentrations for Land Use and Energy. *Science*, (324):1183–1186.
Wolfrom, L. and Yokoi-Arai, M. (2016). Financial Instruments for Managing Disaster Risks Related to Climate Change. *OECD Journal: Financial Market Trends*, 2015(1):25–47.

Figure 2. Term structures of temperature-indexed bond yields and swaps

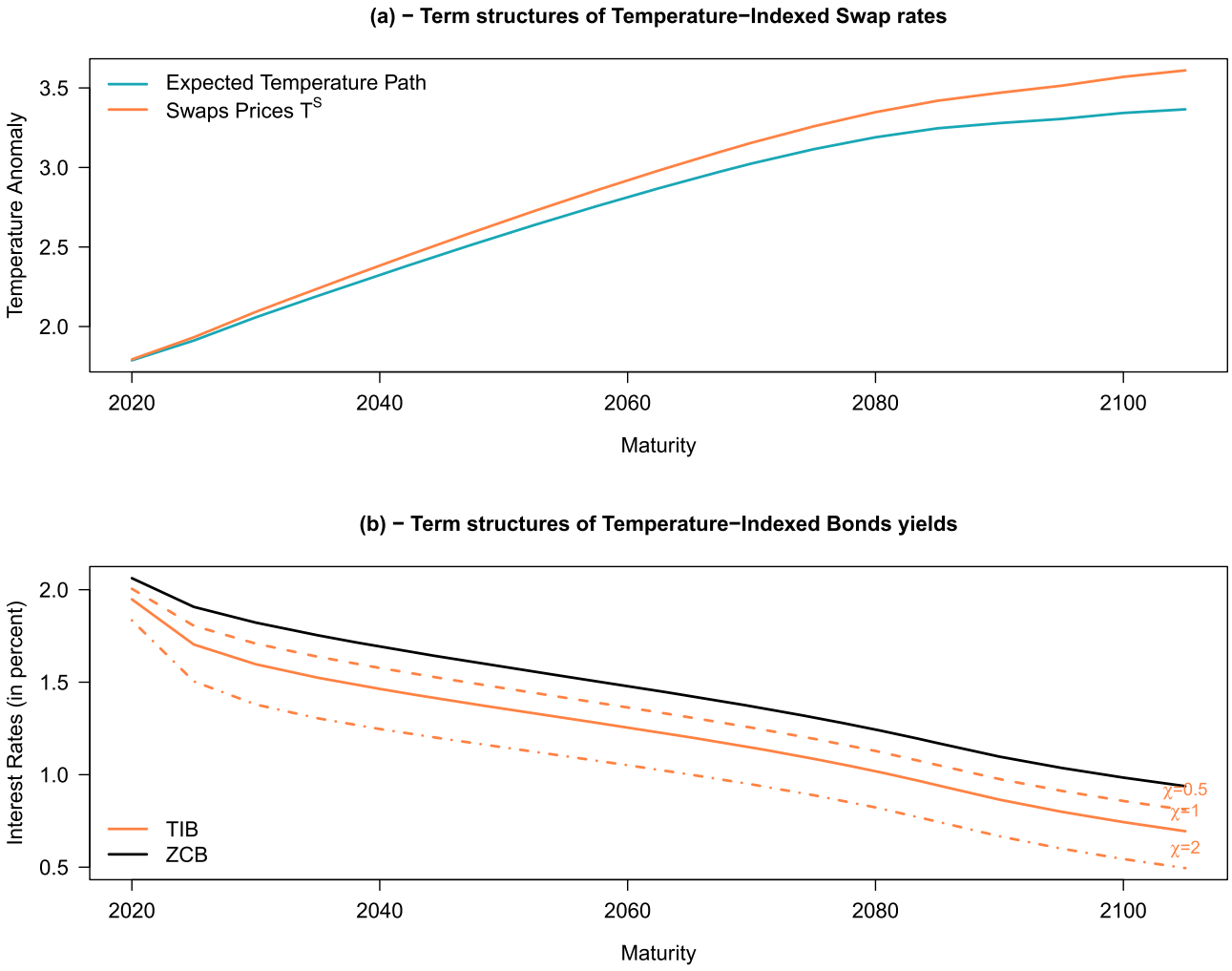

Note: Panel (a) shows the term-structure of temperature-indexed swaps (see Definition 1). More specifically, it shows temperature swap rates ($T^S_{t,h}$) for different maturities h (in orange). The blue line is the expected atmospheric temperature, i.e., $\mathbb{E}_t(T_{AT,t+h})$. If agents were not risk-averse, the orange line would coincide with the blue one; in other words, the deviation between the two lines reflects climate risk premiums. Panel (b) shows the term structure of Temperature-Indexed Bond (TIB) real rates, for different values sensitivity factors χ (see Definition 2). Note that the model does not account for inflation; reported TIB rates therefore are homogenous to real rates. Specifically, denote by $P_{t,h}(\chi)$ the price of this bond, the associated yield-to-maturity (represented by the orange line) is then given by $-\frac{1}{h}\log P_{t,h}(\chi)$. The black line shows yields-to-maturity associated with standard zero-coupon (real) bonds (these yields are given by $-\frac{1}{h}\log \mathbb{E}_t(\mathscr{M}_{t,t+h})$).

Figure 3. Sensitivity of expected temperatures (in 2100) to μ_N and μ_D

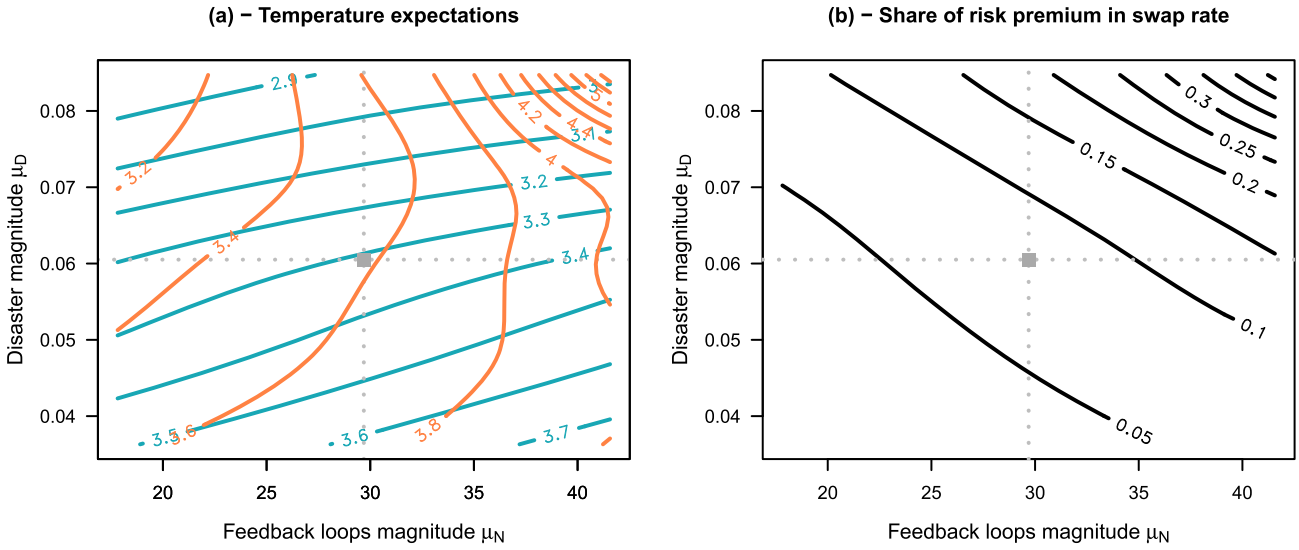

Note: This figure illustrates the sensitivity of $\mathbb{E}_0(T_{AT,2100})$ and $T^S_{0,2100}$ (the Temperature-Indexed Swap of maturity 2100, see eq. (3)) to μ_D and μ_N. The former parameter is the magnitude of climate related disasters (see eq. (28)); the latter is the magnitude of feedback loops (see eq. (29)). On Panel (a), blue lines correspond to expected temperatures ($\mathbb{E}_0(T_{AT,2100})$), and orange lines correspond to temperature swaps ($T^S_{0,2100}$). Panel (b) displays the fraction of the swap price that corresponds to climate risk premiums, i.e., $(T^S_{0,2100} - \mathbb{E}_0(T_{AT,2100}))/T^S_{0,2100}$. The grey squares, in the middle of the plots, locate our baseline calibration.

Figure 4. Sensitivity of temperature risk premiums to μ_N and μ_D

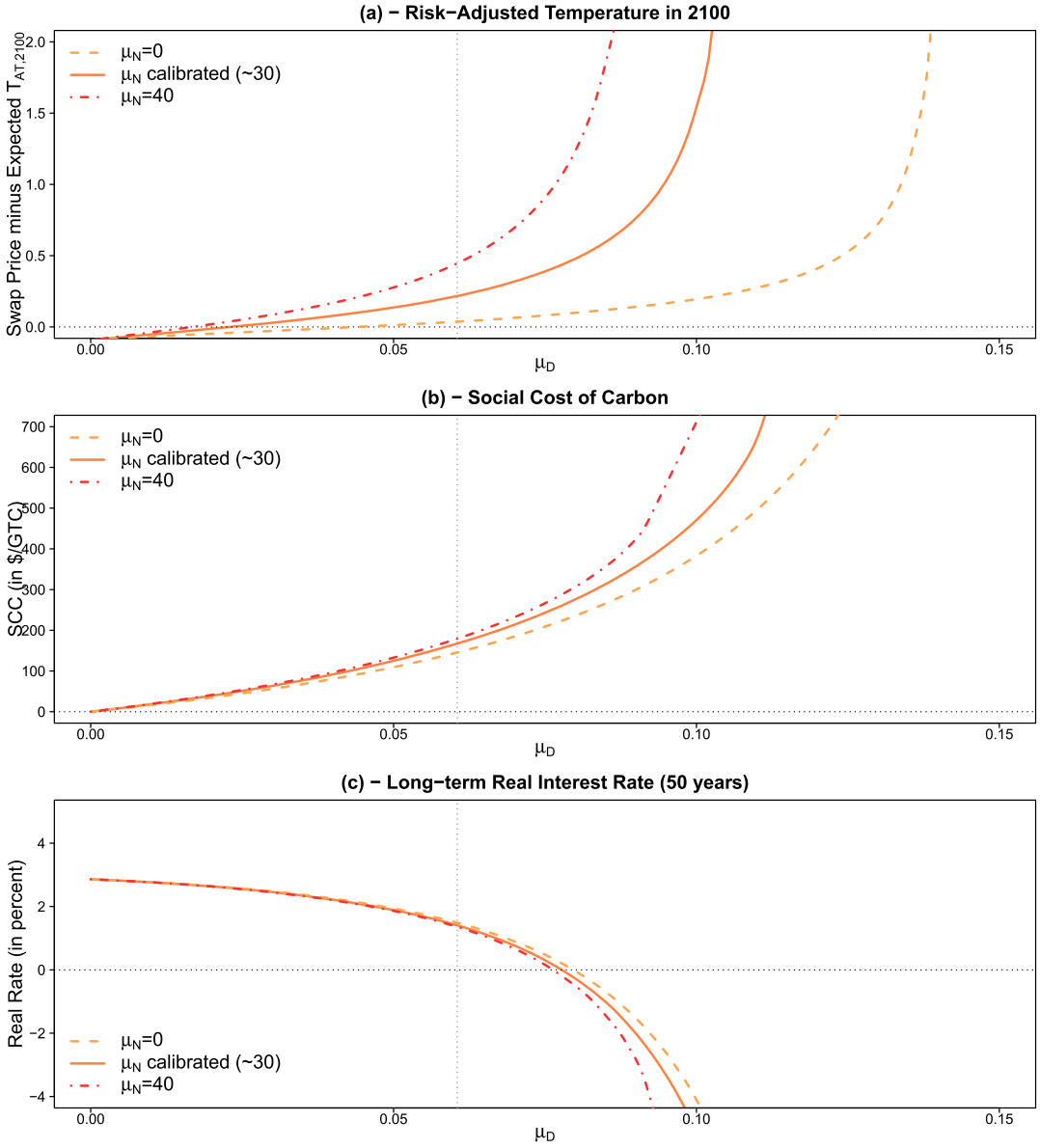

Note: This figure shows the difference between the temperature swap price of maturity 2100 ($T^S_{0,2100}$, see eq. (3)) and expected temperature $\mathbb{E}_0(T_{AT,2100})$. This difference is a risk premium; it would be equal to zero if agents were not risk averse. The plot highlights that this risk premium non linearly depends on μ_D (the magnitude of climate related disasters, see eq. (28)). The two dashed lines are obtained for two different values of the magnitudes of feedback loops (μ_N, see eq. (29)); the solid line uses our baseline (calibrated) value of μ_N. The vertical dashed line locates our baseline (calibrated) value of μ_D.

Figure 5. Conditional distribution of future temperatures (swaps versus physical)

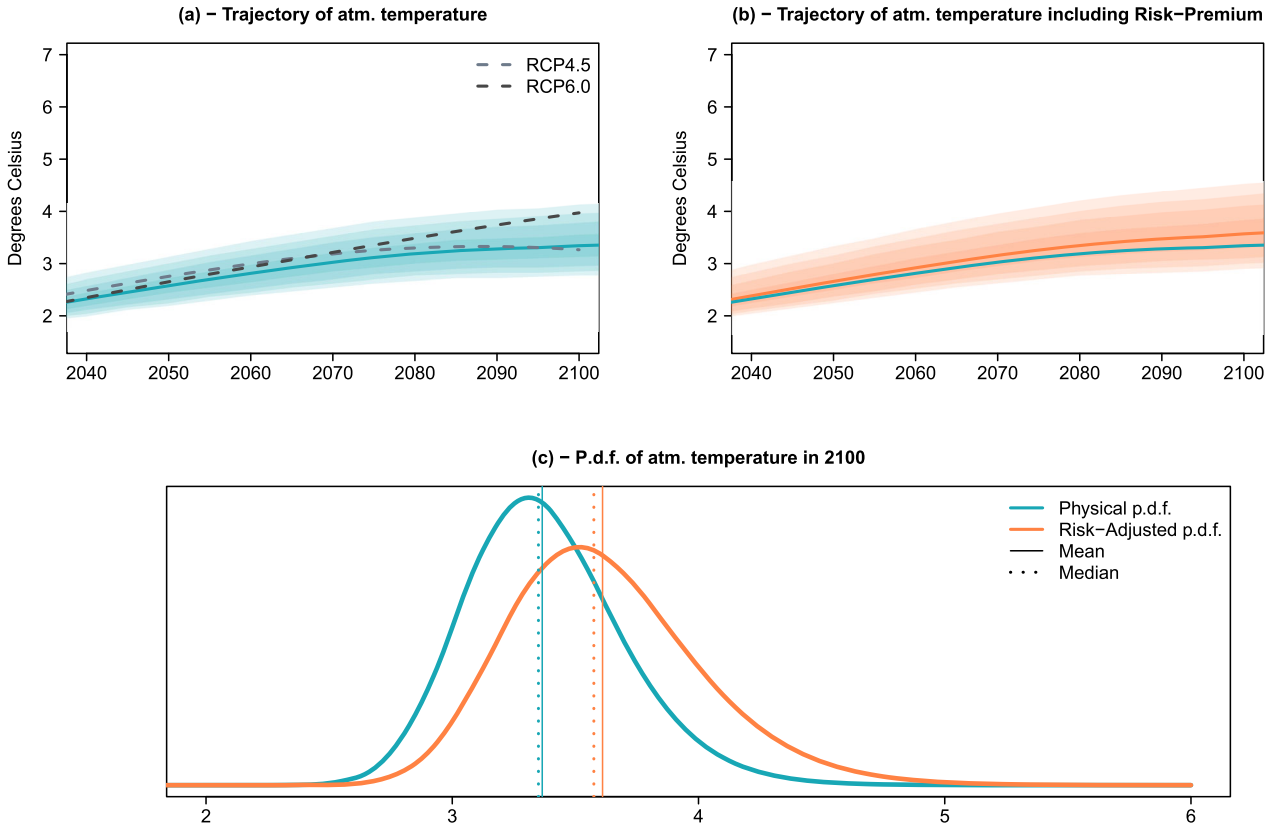

Note: Panel (a) displays the conditional distribution of future atmospheric temperatures. The shaded areas are 50%, 80%, 90%, and 95% confidence intervals. The central blue line shows the medians of the distributions. The dashed lines indicates two IPCC's Representative Concentration Pathway (RCP) scenarios, namely RCP45 and RCP60 (see Footnote 41 for references). The orange solid line in Panel (b) is the term structure of temperature swap prices ($T^S_{0,h}$), that can be seen as risk-adjusted distributions (see Footnote 25 for technical details regarding risk-adjusted probabilities). The shaded areas shown in Panel (b) are 50%, 80%, 90%, and 95% confidence intervals, using risk-adjusted probabilities. Panel (c) shows the conditional distributions of $T_{AT,2100}$ under the physical (blue) and risk-adjusted (orange) measures.

Figure 6. Price of digital options, with contributions of risk premiums

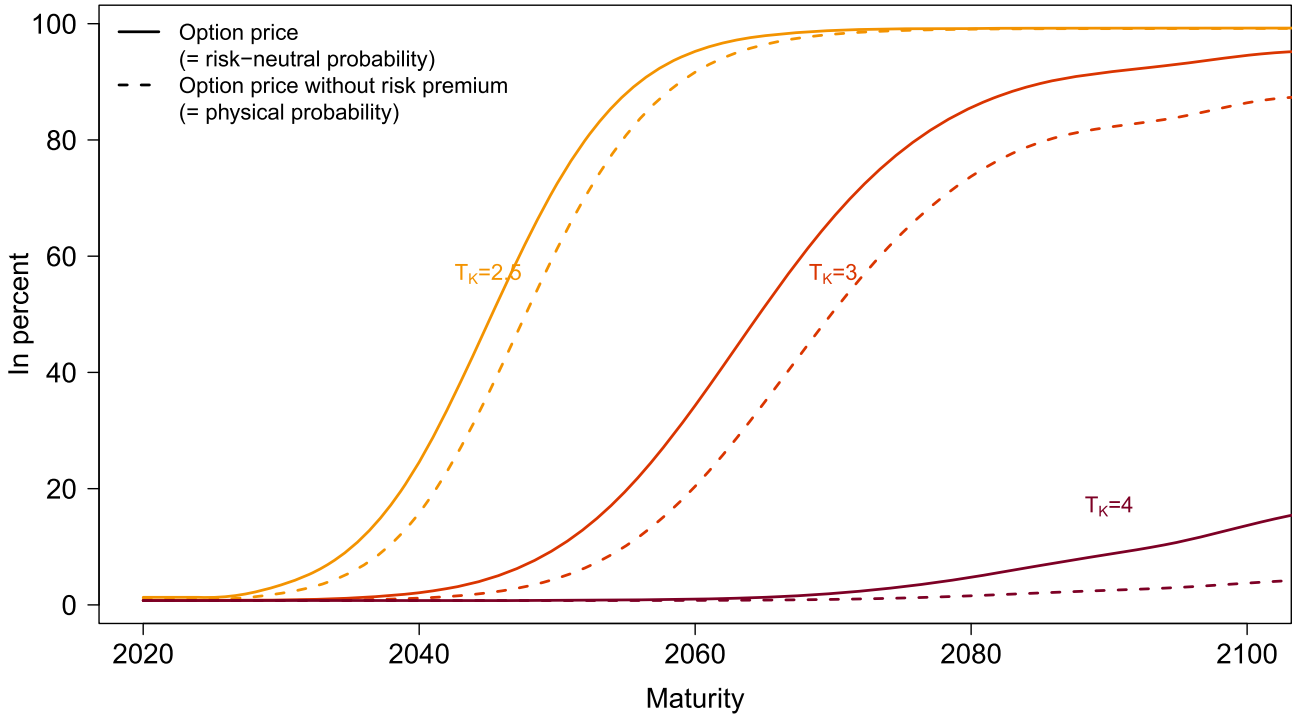

Note: This figure shows the prices of digital options (see Definition 3) for different strikes (T_K) and maturities (x axis). More specifically, the solid lines display, for different maturities (h), $Dig_{t,h}(T_K)/B_{t,h}$, where $Dig_{t,h}$ is the date-t price of an option providing the payoff $\mathbb{1}_{\{T_{AT,t+h}>T_K\}}$ on date $t+h$ (see Definition 3) and $B_{t,h}=\mathbb{E}_t(\mathscr{M}_{t,t+h})$ is the date-t price of a zero-coupon bond of maturity h. The dashed lines show the probabilities that $T_{AT,t+h}>T_K$. If agents were not risk-averse, then solid lines would coincide with dashed lines; in other words, the deviations between solid and dashed lines reflect climate risk premiums.

Figure 7. Conditional distribution of future carbon concentration (swaps versus physical)

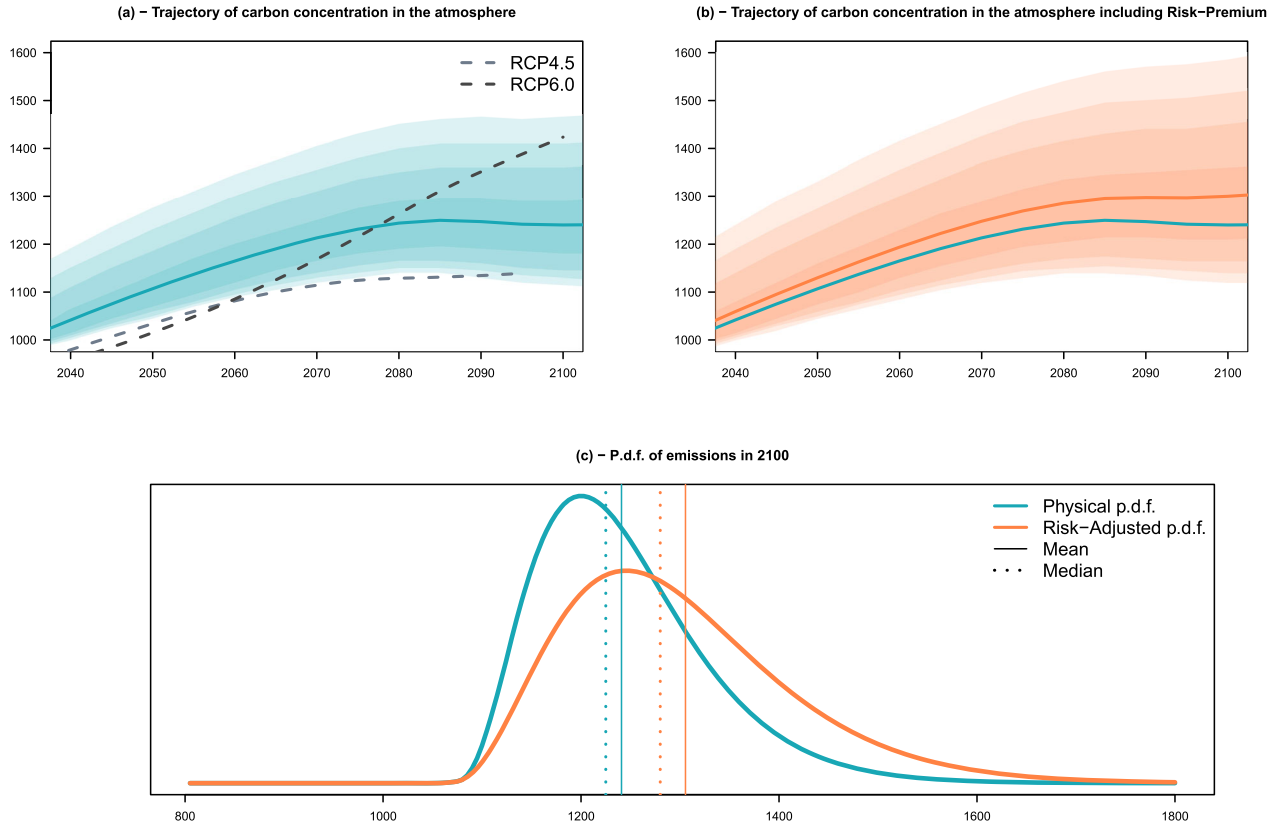

Note: Panel (a) displays the conditional distribution of future atmospheric carbon concentrations. The shaded areas are 50%, 80%, 90%, and 95% confidence intervals. The central blue line shows the medians of the distributions. The dashed lines indicates two IPCC's Representative Concentration Pathway (RCP) scenarios, namely RCP45 and RCP60 (see Footnote 41 for references). The orange solid line in Panel (b) is the term structure of temperature swap prices ($M^S_{0,h}$), that can be seen as risk-adjusted distributions (see Footnote 25 for technical details regarding risk-adjusted probabilities). The shaded areas shown in Panel (b) are 50%, 80%, 90%, and 95% confidence intervals, using risk-adjusted probabilities. Panel (c) shows the conditional distributions of $M_{AT,2100}$ under the physical (blue) and risk-adjusted (orange) measures.

Figure 8. Conditional distribution of future global sea level (swaps versus physical)

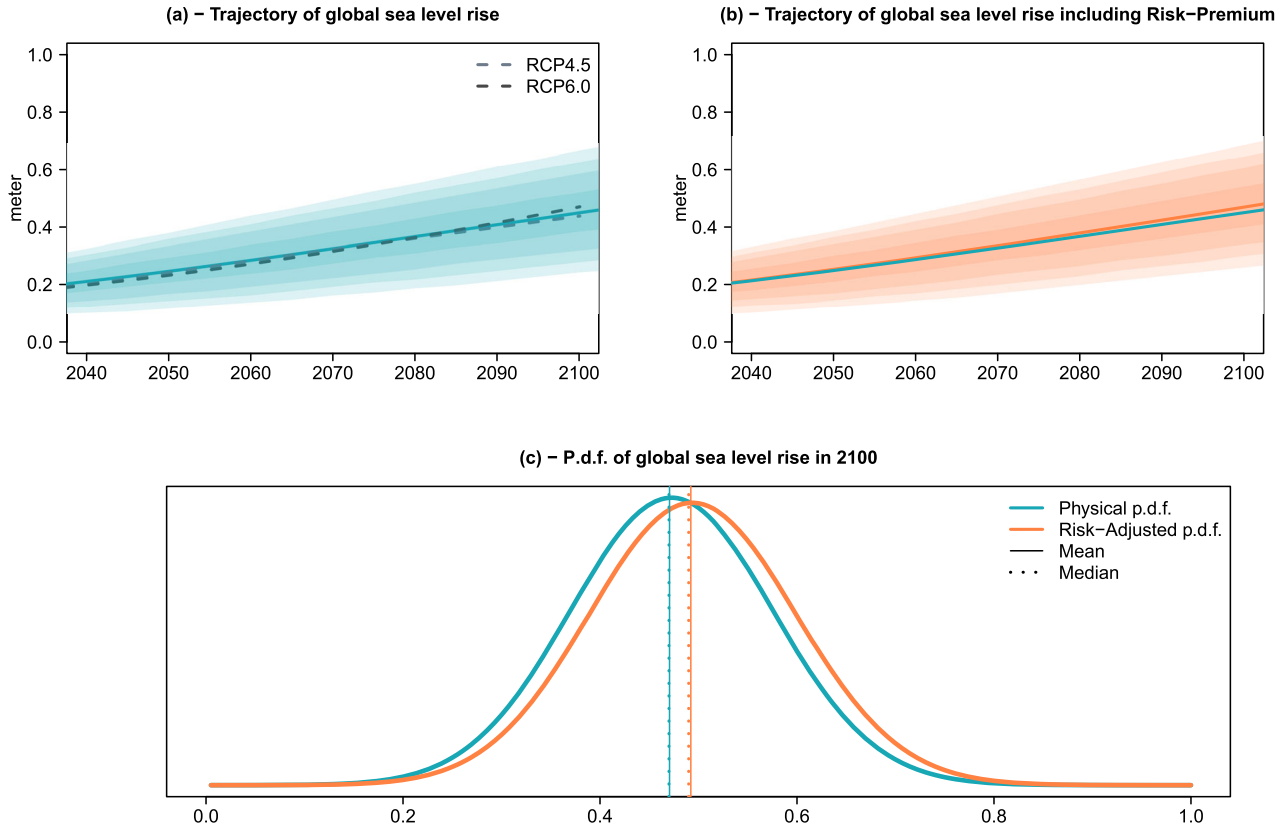

Note: Panel (a) displays the conditional distribution of future global sea level. The shaded areas are 50%, 80%, 90%, and 95% confidence intervals. The central blue line shows the medians of the distributions. The dashed lines indicates two IPCC's Representative Concentration Pathway (RCP) scenarios, namely RCP45 and RCP60 (see Footnote 41 for references). The orange solid line in Panel (b) is the term structure of temperature swap prices ($H^S_{0,h}$), that can be seen as risk-adjusted distributions (see Footnote 25 for technical details regarding risk-adjusted probabilities). The shaded areas shown in Panel (b) are 50%, 80%, 90%, and 95% confidence intervals, using risk-adjusted probabilities. Panel (c) shows the conditional distributions of H_{2100} under the physical (blue) and risk-adjusted (orange) measures.

Figure 9. Social Cost of Carbon (and the contribution of risk premiums)

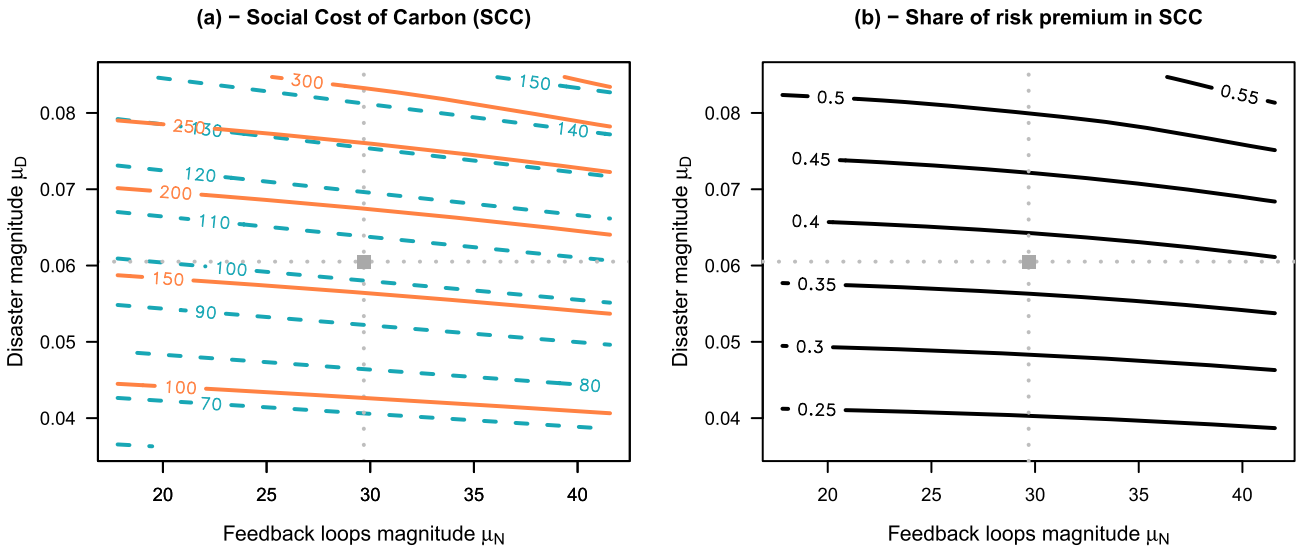

Note: This figure illustrates the sensitivity of the social cost of carbon (SCC, see eq. (43)) to μ_D and μ_N. The former is the magnitude of climate related disasters (see eq. (28)); the latter is the magnitude of feedback loops (see eq. (29)). On Panel (a), dashed lines correspond to the SCC that would prevail under the expectation hypothesis, i.e., if agents were risk-neutral. Panel (b) displays the fraction of the SCC corresponding to climate risk premiums. The risk premium is given by the difference between the risk-adjusted prices (in orange in Panel (a)) and the price that would prevail under the expectation hypothesis (in blue in Panel (a)). The grey squares, in the middle of the plots, locate our baseline calibration.

A Model

A.1 Exogenous equations

Carbon intensity:

$$\sigma_t = \sigma_{t-1}(1+g_{\sigma,t}), \text{ with } g_{\sigma,t} = g_{\sigma,t-1}(1+\delta_\sigma)^{\Delta t}. \tag{18}$$

Emission reduction rate (equivalent to (14)):

$$\mu_t = \min\left[\exp\left(-\left|\theta_{a,opt}\right| + \left|\theta_{b,opt}\right| \times t\right); 1\right], \tag{19}$$

where $\left|\theta_{a,opt}\right| > \left|\theta_{b,opt}\right| T^*$, with $T^* = 12$. This last inequality ensures that complete mitigation is not obtained before 2080 ($T^* = 12$).

Backstop price:

$$BP_t = pback(1-gback)^{t-1}. \tag{20}$$

Adjusted cost for backstop:

$$BC_t = \frac{BP_t \sigma_t}{1000 \times \theta_2}. \tag{21}$$

Exogenous land emissions:

$$\mathscr{E}_{Land,t} = \varepsilon_0(1-\rho)^{t-1}. \tag{22}$$

Exogenous radiative forcings:

$$F_{EX,t} = \begin{cases} \phi_0 + \frac{1}{17}(\phi_1 - \phi_0)(t-1) & \text{if } t < 18 \quad (t = 18 \text{ corresponds to } 2100) \\ \phi_1 & \text{if } t \geq 18. \end{cases} \tag{23}$$

Abatement costs:

$$\Lambda_t = \mu_t^{\theta_2} BC_t. \tag{24}$$

A.2 Endogenous equations

As shown in Online Appendix I.1, under the assumptions described in Section 4, consumption growth is given by (this is (15)):

$$\Delta c_t = \mu_{c,t} + \sigma_{c,t}\eta_{A,t} - D_t, \tag{25}$$

where $\mu_{c,t}$ and $\sigma_{c,t}$ are given by

$$\begin{cases} \mu_{c,t} &= \log\delta + \log\left((1-\Lambda_t)\bar{A} + (1-dep)\right) \\ \sigma_{c,t} &= \frac{(1-\Lambda_t)}{(1-\Lambda_t)\bar{A}+(1-dep)}\sigma_A, \end{cases} \tag{26}$$

and where $\eta_{A,t}$ is a component of vector η_t, which follows a Gaussian Vector Auto-Regressive (VAR) process of order one:

$$\eta_t = \Phi\eta_{t-1} + \varepsilon_{\eta,t}, \quad \text{with } \mathbb{V}\text{ar}(\varepsilon_{\eta,t}) = \Sigma_{\eta,t} = \mathbf{Id}_{n_\eta \times n_\eta}. \tag{27}$$

Industrial damages (affecting productive capital, see (12)):

$$D_t = \gamma_0\left(\ell_0^{(D)} + \ell_1^{(D)} T_{AT,t-1}, \mu_D\right), \tag{28}$$

where γ_0 denotes the gamma-zero distribution (Monfort et al., 2017). This distribution features a Dirac mass at zero. Specifically, the probability of having $D_t = 0$ is equal to $\exp(-\ell_0^{(D)} - \ell_1^{(D)} T_{AT,t-1})$.

Carbon release - Feedback effect:

$$N_t = \gamma_0\left(\frac{\rho_N}{\mu_N} N_{t-1} + \ell_0^{(N)} + \ell_1^{(N)} T_{AT,t-1}, \mu_N\right). \tag{29}$$

Up to potential mitigation (μ_t, see Section 4) and to deterministic decrease in the carbon intensity of production σ_t (see eq. 18), industrial carbon emissions are supposed to grow as (planned) capital. This leads to (see Online Appendix I.2):

$$\mathscr{E}_{Ind,t} = \sigma_t(1-\mu_t) q_0 \exp\left(\sum_{i=1}^{t}\left[\mu_{c,i} + \frac{1}{2}\sigma_{c,i}^2\right]\right)\left[1 + \tilde{y}_{t-1}\right], \tag{30}$$

where

$$\tilde{y}_t = \sum_{i=1}^{t} \sigma_{c,i}\eta_{A,i}. \tag{31}$$

Total emissions (equivalent to (8)):

$$\mathscr{E}_t = \mathscr{E}_{Land,t} + \mathscr{E}_{Ind,t} + N_t. \tag{32}$$

Radiative forcing (equivalent to (6), see also Online Appendix IV.1):

$$F_t = \tau \log_2(m_0) + \frac{\tau}{\log(2) m_0}\left(\frac{M_{AT,t}}{M_{PI}} - m_0\right) + F_{EX,t} + \sigma_F \eta_{F,t} \tag{33}$$

where $\eta_{F,t}$ is a component of vector η_t (see equation (27)).

Carbon cycle - carbon concentration increase (equivalent to (7)):

$$\begin{bmatrix} M_{AT,t} \\ M_{UP,t} \\ M_{LO,t} \end{bmatrix} = \begin{bmatrix} \varphi_{11} = 1 - \varphi_{12} & \varphi_{21} = \varphi_{12}\frac{mateq}{mueq} & 0 \\ \varphi_{12} & \varphi_{22} = 1 - \varphi_{21} - \varphi_{23} & \varphi_{32} = \varphi_{23}\frac{mueq}{mleq} \\ 0 & \varphi_{23} & \varphi_{33} = 1 - \varphi_{32} \end{bmatrix}^5 \begin{bmatrix} M_{AT,t-1} \\ M_{UP,t-1} \\ M_{LO,t-1} \end{bmatrix} + \frac{\Delta t}{3.666}\begin{bmatrix} \mathscr{E}_{t-1} \\ 0 \\ 0 \end{bmatrix}. \tag{34}$$

Temperature increase in the atmosphere (equivalent to (5)):

$$T_{AT,t} = T_{AT,t-1} + \xi_1 \left\{ F_t - \frac{\tau}{\nu} T_{AT,t-1} - \xi_2 \left[T_{AT,t-1} - T_{LO,t-1} \right] \right\}. \tag{35}$$

Temperature increase in the ocean:

$$T_{LO,t} = T_{LO,t-1} + \xi_3 \left\{ T_{AT,t-1} - T_{LO,t-1} \right\}. \tag{36}$$

Sea level increase (equivalent to (9)):

$$H_t = H_{t-1} + \Delta t \times a_{SAT} (T_{AT,t} - T_{0,S}) + b_{SAT} \Delta T_{AT,t} + \sigma_H \eta_{H,t}. \tag{37}$$

A.3 Agents' preferences

We consider an agent featuring Epstein and Zin (1989) preferences, with a unit elasticity of intertemporal substitution (EIS).[46] Specifically, the time-t utility of a consumption stream (C_t) is recursively defined by:

$$u_t = (1-\delta) c_t + \frac{\delta}{1-\gamma} \log \left(\mathbb{E}_t \exp \left[(1-\gamma) u_{t+1} \right] \right), \tag{38}$$

where c_t denotes the logarithm of the agent's consumption level C_t, δ the time discount factor and γ the risk aversion parameter.[47]

Online Appendix I.1 shows that, in the economy described in Section 4, the log consumption growth, that is $\Delta c_t = c_t - c_{t-1}$, is of the form $\mu_{c,t} + \sigma_{c,t} \eta_{A,t} - D_t$ (that is eq. 15, with $\mu_{c,t}$ and $\sigma_{c,t}$ given by eq. 26). Online Appendix II further shows that the model admits a state-space representation where the state vector X_t includes, in particular, $\eta_{A,t}$ and D_t (see eq. II.1). Accordingly, Δc_t is affine in X_t, that is:

$$\Delta c_t = c_t - c_{t-1} = \mu_{c,0,t} + \mu'_{c,1,t} X_t, \tag{39}$$

where $\mu_{c,0,t}$ and $\mu_{c,1,t}$ are deterministic processes. Moreover, Online Appendix II shows that X_t admits an exponential affine log-Laplace transform:

$$\psi_t(u, X_t) := \log \mathbb{E}_t (\exp(u' X_{t+1})) = \alpha_t(u) + \beta_t(u)' X_t, \tag{40}$$

where functions α_t and β_t are deterministic (eq. II.6).

Appendix III.1 shows that, in this context, the s.d.f. is given by:

$$M_{t,t+1} = \exp \left[-(\eta_{0,t} + \eta'_{1,t} X_t) + \pi'_t X_{t+1} - \psi_t(\pi_t, X_t) \right], \tag{41}$$

where the vector of prices of risk π_t as well as $\eta_{0,t}$ and $\eta_{1,t}$ are deterministic objects whose computation is detailed in Proposition 9 (Appendix III.1).

[46] Using a unit EIS facilitates resolution (Piazzesi and Schneider, 2007). In an IAM context, Hambel et al. (2021) also work under the assumption of a unit EIS. This value is however slightly below the lower bound of the 90% confidence interval found by Schorfheide et al. (2018). Daniel et al. (2019) take an EIS of 0.9.

[47] Eq. (38) results from a first-order Taylor expansion around $\rho = 1$ of the general Epstein and Zin (1989) recursive utility defined by: $u_t = \frac{1}{1-\rho} \log \left((1-\delta) C_t^{1-\rho} + \delta \left(\mathbb{E}_t \left[\exp\{(1-\gamma) u_{t+1}\} \right] \right)^{\frac{1-\rho}{1-\gamma}} \right)$, where ρ is the inverse of the EIS.

B Calibration

Most of the model parameters are directly borrowed from the literature (see Table 4), and in particular from DICE16 (Nordhaus, 2017). Additional parameters, that are more specific to the model used in this paper, are calibrated in such a way as to make the model-implied dynamics of our model consistent with different moments found in the literature (see Table 1). In practice, this is achieved by minimizing a loss function expressing the deviation between targeted and model-implied moments. Formally, define by γ the vector of targeted moments, by θ the vector of (free) parameters, and by $\psi(\theta)$ the model-implied moments. The calibrated parameters $\widehat{\theta}$ solve for the following optimization problem:

$$\widehat{\theta} = \underset{\theta}{\operatorname{argmin}} \, (\gamma - \psi(\theta))' \Omega (\gamma - \psi(\theta)), \tag{42}$$

where Ω is a diagonal matrix whose diagonal entries are weights associated with the different moments we consider. Alternatively put, $(\gamma - \psi(\theta))' \Omega (\gamma - \psi(\theta))$ is a loss function that is minimized for $\theta = \widehat{\theta}$.

Table 2 shows the parameters resulting from this moment-fitting approach.

Table 1. Targeted and model-implied moments (in 2100)

Moment	Target	Model-implied	Source
Expectation of $T_{AT,2100}$	3.50°C	3.34°C	RCP4.5+RCP6.0
Standard deviation of $T_{AT,2100}$	0.25°C	0.32°C	RCP4.5+RCP6.0
Expected contribution of FL to GMST	0.25°C	0.27°C	Burke et al. (2012)
Expected increase in cumulated emissions due to FL	188 $GtCO_2$	189 $GtCO_2$	Burke et al. (2012)
Linear regression slope of cumulated damages on GMST	−0.12	−0.12	Burke et al. (2015b)
Long-term rate target	1.00%	0.94%	US Treasury
$\mathbb{E}(H_{2100})$	0.45m	0.45m	RCP4.5+RCP6.0
Standard Deviation of H_{2100}	0.10m	0.10m	Mengel et al. (2016)

Note: This table compares targeted and model-implied moments, after having minimized a loss function that reflects the distance between these two sets of moments. Resulting parameters are shown in Table 2. All moments are for 2100 and are conditional on the information available on date $t = 0$ (that is 2015). FL stands for "Feedback Loops" (see Section 4). Numbers for FL targets are in line with alternative estimations (Schaefer et al., 2014). Temperatures anomalies in Representative Concentration Pathway (RCP) scenarios are expressed relative to the 1850-1900 baseline period (IPCC, 2014). RCP scenarios are based on Clarke et al. (2007); Smith and Wigley (2006); Wise et al. (2009); Fujino et al. (2006); Hijioka et al. (2008). The targeted linear regression slope of cumulated emissions due to FL is based on Figure 5.d in Burke et al. (2015b), which shows that a four-unit increase in Global mean surface temperature (GMST) implies a 50% reduction in GDP per capita; the model-implied equivalent, i.e. the population regression coefficient, is given by $\mathbb{C}ov_{t=0}(Cum_{D,t=2100}, T_{t=2100})/\mathbb{V}ar_{t=0}(T_{t=2100})$, where $Cum_{D,t=2100}$ is the cumulated consumption loss stemming from climate-related disasters between the current date and 2100. (Note that the population regression coefficient, which depends only on second-order moments, is available in closed-form in our framework.) The long term rate target is based on the High Quality Market (HQM) corporate bond yield curves. These very-long-term yields are computed by the U.S. Department of the Treasury for the Pension Protection Act. The 100-year rate is available at `https://fred.stlouisfed.org/series/HQMCB100YR`. This nominal rate is currently around 4%; we set our real rate target at 1%, which is consistent with an inflation rate assumption of 2% and a credit spread of 100 basis points (as the rates reported by the Treasury corresponds to corporate—hence defaultable—bonds). Including the very-long-term real rate among the targets has the advantage of discarding calibrations for which long-term bonds have infinite prices. (The fact that long-term rates may not exist is not specific to the present model.)

Table 2. Estimated parameters

Parameter	Notation	Equation	Value	Unit/Note
Average TFP	$\bar{A}$	(28)	0.43	
Standard deviation of TFP shock	σ_A	(28)	3.33	
Size of disasters	μ_D	(28)	6.05	%
Constant term in damage specification	ℓ_0^D	(28)	0.00	
Slope coefficient in damage specification	ℓ_1^D	(28)	0.19	
Size of carbon releases	μ_N	(29)	29.69	$GtCO_2$
Constant term in carbon-release specification	ℓ_0^N	(29)	0.10	
Slope coefficient in carbon-release specification	ℓ_1^N	(29)	0.10	
Auto-correlation of carbon releases	ρ_N	(29)	0.00	
Standard deviation radiative forcings shock	$\sigma_{\eta,F}$	(33)	0.31	
Backstop price	$pback$	(20)	2488	\$
Sea level coefficient on $\Delta_{(T_{AT},T_{0,S})}$	a_{SAT}	(37)	0.0013	\$
Sea level shock	σ_H	(37)	0.0233	\$

Note: This table presents the parameters obtained by minimizing a loss function measuring the distance between model-implied and targeted moments (see Table 1).

Table 3. Initial values of state vector X_0

Variable	Notation	Value	Reference
Initial consumption growth	Δc_0	9.71%	CDICE
Initial cumulative TFP shocks	$\tilde{y}_0$	0.00	
Initial emissions	$\mathscr{E}_0$	$38.45GtCO_2$	CDICE
Initial industrial emissions	$E_{ind,0}$	$35.85GtCO_2$	CDICE
Initial radiative forcings	F_0	$2.00W/m^2$	CDICE
Initial carbon concentration (atmos.)	$M_{AT,0}$	850.00GtC	CDICE
Initial carbon concentration (upper ocean)	$M_{UP,0}$	765.00GtC	CDICE
Initial carbon concentration (lower ocean)	$M_{LO,0}$	1799.00GtC	CDICE
Initial temperature anomaly (atmos.)	$T_{AT,0}$	1.28°C	CDICE
Initial temperature anomaly (lower ocean)	$T_{LO,0}$	0.31°C	CDICE
Cumulative damages	$Cum_{D,0}$	0.00%	CDICE
Cumulative emissions	$Cum_{\mathscr{E},0}$	$0.00GtCO_2$	CDICE
Cumulative consumption growth	$Cum_{\Delta c,0}$	9.71%	CDICE
Initial sea level	H_0	0.13m	Vermeer and Rahmstorf (2009)

Table 4. Calibrated parameters (period = 5 years)

Parameter	Notation	Equation	Value	Unit/Note	Reference
Value of $M_{AT,t}/M_{PI}$ used in the linearization of (IV.1)	m_0	(33)	$\frac{1168}{607}$		CDICE + IPCC
Rate of preference for present	δ	(38)	0.95		
Risk aversion	γ	(38)	7		
Carbon emissions from land 2015	ε_0	(22)	2.6	$GtCO_2$ per year	DICE2016
Decline rate in land emissions (Eq. 22)	ρ	(22)	0.115	per period	DICE2016
Equilibrium concentration in atmosphere	$mateq$	(34)	607	GtC	CDICE
Equilibrium concentration in upper strata	$mueq$	(34)	600	GtC	CDICE
Equilibrium concentration in lower strata	$mleq$	(34)	1772	GtC	CDICE
2015 forcings of non-CO_2 GHG	ϕ_0	(23)	0.5	W/m^2	DICE2016
2100 forcings of non-CO_2 GHG	ϕ_1	(23)	1	W/m^2	DICE2016
Preindustrial concentration of carbon in the atmosphere	M_{PI}	(33)	607	GtC	CDICE
Carbon cycle parameter between atmosphere and upper ocean	φ_{12}	(34)	0.053		CDICE
Carbon cycle parameter between upper and lower ocean	φ_{23}	(34)	0.0042		CDICE
Climate equation coefficient for upper level	ξ_1	(35)	$\Delta t \times 0.137$		CDICE
Transfer coefficient upper to lower stratum	ξ_2	(35)	$\Delta t \times 0.10001$		CDICE
Transfer coefficient for lower level	ξ_3	(36)	$\Delta t \times 0.00689$		CDICE
Forcings of equilibrium CO_2 doubling	τ	(33)+(35)	3.45	W/m^2	CDICE
Equilibrium temperature impact	ν	(35)	3.25	°C per doubling CO_2	CDICE
Decline rate of decarbonization	δ_σ	(18)	-0.001	per period	DICE2016
Carbon intensity 2010	σ_0	(18)	$\frac{e_0}{q_0(1-\mu_0)}$	$kgCO_2$ per output 2005 USD 2010	DICE2016
Industrial emissions in 2015	e_0	$(\sigma_0)+(\mathscr{E}_{2015})$	35.85	$GtCO_2$ per year	DICE2016
Initial world gross output in 2015	q_0	(30)+(σ_0)	105.5	trillions of 2010 USD	DICE2016
Initial emision control rate in 2015	μ_0	(19)	0.03		DICE2016
Initial growth of sigma	$g_{\sigma,1}$	(18)	-0.0152	per year	DICE2016
Initial cost decline backstop cost	$gback$	(20)	0.025	per period	DICE2016
Exponent of control cost function	θ_2	(21)+(24)	2.6		DICE2016
Persistence of the radiative forcings shock	$\Phi_{[2,2]}$	(27)	0.95		
Global surface temperature weights [T_{AT}, T_{LO}]	$weights_T$		$[0.6, 0.4]$		IPCC
Base Temperature (sea level equilibrium)	$T_{0,S}$	(37)	-0.375	°C, Baseline [1951-1980]	Vermeer and Rahmstorf (2009)
Coefficient attached to $\Delta T_{AT,t}$	b_{SAT}	(37)	0.025	m	Vermeer and Rahmstorf (2009)
Capital depreciation rate	dep	(I.7)	0.27		
Time step	Δt		5		

Note: This table presents the parameters used in our baseline model. DICE16 refers to Nordhaus (2017). IPCC refers to IPCC (2014, Table 2.1). CDICE refers to Folini et al. (2021)

C Social cost of carbon

In this subsection, we examine the model-implied Social Cost of Carbon (SCC) and the influence risk premiums have on this measure of economic costs of carbon emissions. Following the literature, we define the SCC as the marginal rate of substitution between atmospheric carbon concentration and consumption, that is:

$$SCC_t = -\frac{\partial U_t}{\partial M_{AT,t}} \Big/ \frac{\partial U_t}{\partial C_t}. \tag{43}$$

In our framework, the SCC is available in closed-form (Online Appendix III.3). Table 5 shows how our baseline SCC estimate (of \$167 per tC) compares to those obtained in alternative studies.

Figure 9 depicts how the SCC depends on the two key parameters that are μ_D (magnitude of climate-related disasters) and μ_D (magnitude of adverse feedback loops). On Panel (a), the orange lines show the model-implied SCC. We observe that the SCC is particularly sensitive to the average disaster size (μ_D). On the same panel, the blue lines indicate the SCC that would prevail if agents were not risk-averse. Our results suggest that risk aversion has a strong influence on SCC or, alternatively put, risk premiums account for a large share of the SCC. For the baseline calibration of μ_D and μ_N (see the central point of the plot), risk premiums account for more than half of the SCC. Panel (b) further shows that this share positively depends on both μ_D and μ_N.

[Insert Figure 9 about here]

Table 5. SCC comparison

Study	SCC (U.S. \$ per tC)	Tipping points	Stochastic IAM	Discount Rate
Nordhaus (2017)	113			1.5%
Stern (2007)	312			0%
Jensen and Traeger (2014)	[40;70]		✓	1.5%
Barnett et al. (2020)	[240;411]		✓	1%
Cai and Lontzek (2019)	[40;100]	✓	✓	1.5%
Bansal et al. (2016)	[4;104]	✓	✓	1%
Lemoine and Traeger (2014)	[37;55]	✓	✓	1.5%
van den Bremer and van der Ploeg (2021)	146		✓	1.5%
This paper	167	✓	✓	1%

Note: This table reports different SCC estimates. Cited studies differ along many dimensions, the last three columns highlight particularly important ones.

—Online Appendix—

Climate Linkers: Rationale and Pricing

Pauline CHIKHANI and Jean-Paul RENNE

I Consumption and emission growth rates in the production economy

I.1 Solving for the consumption process

In this appendix, we derive the consumption growth process in our production economy. Let us denote agents' wealth by $\mathscr{W}_t$. In the context of Epstein-Zin-Weil preferences, and with a unit Elasticity of Intertemporal Substitution, it can be shown that:[48]

$$C_t = (1-\delta)\mathscr{W}_t. \tag{I.1}$$

Since agents' wealth at time t is $\mathscr{W}_t = C_t + K^*_{t+1}$, it comes, using (I.1), that:

$$\delta\mathscr{W}_t = K^*_{t+1}, \tag{I.2}$$

Eq. (I.1) then gives:

$$C_t = \frac{1-\delta}{\delta}K^*_{t+1} \tag{I.3}$$

We have:

$$Y_t = C_t + Inv_t + \Psi_t, \tag{I.4}$$

where, Ψ_t, the investment in low-carbon technologies, is given by $\Psi_t = \Lambda_t Y_t$.

On date $t+1$, we have $Y_{t+1} = A_{t+1}K_{t+1}$, which implies that (I.4) rewrites (for date $t+1$):

$$C_{t+1} = (1-\Lambda_{t+1})A_{t+1}K_{t+1} - Inv_{t+1} \tag{I.5}$$

Using (I.3) in $K^*_{t+1} = (1-dep)K_t + Inv_t$ gives:

$$Inv_t = \frac{\delta}{1-\delta}C_t - (1-dep)K_t. \tag{I.6}$$

Using the previous expression in (I.5) yields

$$C_{t+1} = (1-\Lambda_{t+1})A_{t+1}K_{t+1} - \frac{\delta}{1-\delta}C_{t+1} + (1-dep)K_{t+1},$$

[48] See, e.g., Appendix B in Giovannini and Weil (1989).

that is, using $K_{t+1} = \exp(-D_{t+1})K^*_{t+1}$, and (I.3):

$$\frac{1}{1-\delta}C_{t+1} = \Big((1-\Lambda_{t+1})A_{t+1} + (1-dep)\Big)\exp(-D_{t+1})\frac{\delta}{1-\delta}C_t.$$

Finally:

$$\frac{C_{t+1}}{C_t} = \delta\Big((1-\Lambda_{t+1})A_{t+1} + (1-dep)\Big)\exp(-D_{t+1}).$$

Assuming that $A_t = \bar{A} + \sigma_A \eta_{A,t}$, we get:

$$\frac{C_{t+1}}{C_t} = \delta\Big((1-\Lambda_{t+1})(\bar{A} + \sigma_A \eta_{A,t+1}) + (1-dep)\Big)\exp(-D_{t+1}).$$

The resulting log growth rate of consumption is:

$$\begin{aligned}\Delta c_{t+1} &= \log\delta + \log\Big((1-\Lambda_{t+1})(\bar{A} + \sigma_A \eta_{A,t+1}) + (1-dep)\Big) - D_{t+1} \\ &\approx \mu_{c,t+1} + \sigma_{c,t+1}\eta_{A,t+1} - D_{t+1},\end{aligned} \tag{I.7}$$

where $\mu_{c,t}$ and $\sigma_{c,t}$ are given by (26). This is (15).

I.2 Emission growth rate

This subsection explains the specification of industrial emissions, namely eqs. (30) and (31).

Up to potential mitigation (μ_t, see Section 4) and to deterministic decrease in the carbon intensity of production σ_t (see eq. 18), industrial carbon emissions are supposed to grow as (planned) capital. More precisely, as in the DICE framework, industrial carbon emissions of date t are of the form $\sigma_t(1-\mu_t)q_t$, where q_t follows:

$$\frac{q_{t+1}}{q_t} = \frac{K^*_{t+1}}{K_t}.$$

Using $K^*_{t+1} = \frac{1-\delta}{\delta}C_t$ (eq. I.3) and $K_t = \exp(-D_t)K^*_t = \exp(-D_t)\frac{1-\delta}{\delta}C_{t-1}$, we obtain:

$$\frac{q_{t+1}}{q_t} = \frac{C_t}{C_{t-1}}\exp(D_t).$$

Using (I.7), it comes that the log growth rate of q_t is approximately equal to $\mu_{c,t} + \sigma_{c,t}\eta_{A,t}$ (with a one-period lag). This would lead to the following expression for industrial emissions:

$$E_{ind,t} = \sigma_t(1-\mu_t)q_0\exp\left(\sum_{i=1}^{t-1}[\mu_{c,i} + \sigma_{c,i}\eta_{A,t}]\right).$$

However, to preserve the conditional affine property of the model dynamics, industrial emissions have to linearly depend on the shocks $\eta_{A,t}$. Using (a) that $\exp(\mu+\sigma\varepsilon) \approx \exp(\mu+\frac{\sigma^2}{2})(1+\sigma\varepsilon)$ when $\varepsilon \sim \mathcal{N}(0,1)$ and for a small σ, and (b) that the $\eta_{A,t}$s are i.i.d., we get the following expression for industrial emissions:

$$\mathscr{E}_{Ind,t} = \sigma_t(1-\mu_t)q_0\exp\left(\sum_{i=1}^{t}\left(\mu_{c,i} + \frac{\sigma^2_{c,i}}{2}\right)\right)(1+\tilde{y}_{t-1}), \tag{I.8}$$

(that is eq. 30), with $\tilde{y}_t = \sum_{i=1}^{t} \sigma_{c,i}\eta_{A,i}$ (that is eq. 31). Equation (I.8) can also be written as:

$$\mathscr{E}_{Ind,t} = \kappa_t \left(1 + \tilde{y}_{t-1}\right), \tag{I.9}$$

with:

$$\kappa_t = \sigma_t(1-\mu_t)q_0 \exp\left(\sum_{i=1}^{t}\left(\mu_{c,i} + \frac{\sigma_{c,i}^2}{2}\right)\right). \tag{I.10}$$

II State vector's conditional moments and Laplace transform

II.1 Rewriting the model in matrix form

We decompose the state variable, denoted by X_t, as follows:

$$X_t = \begin{bmatrix} Z_t \\ W_t \end{bmatrix}, \quad \text{where} \quad Z_t = \begin{bmatrix} \Delta c_t \\ \tilde{y}_t \\ \mathscr{E}_t \\ \mathscr{E}_{Ind,t} \\ F_t \\ M_{AT,t} \\ M_{UP,t} \\ M_{LO,t} \\ T_{AT,t} \\ T_{LO,t} \\ Cum_{D,t} \\ Cum_{\mathscr{E},t} \\ Cum_{\Delta c,t} \\ H_t \end{bmatrix}, \quad \text{and } W_t = \begin{bmatrix} \eta_{t,[3\times 1]} \\ D_t \\ N_t \end{bmatrix}, \tag{II.1}$$

where $Cum_{D,t} = -\sum_{i=1}^{t} D_i$, $Cum_{\mathscr{E},t} = \sum_{i=1}^{t} \mathscr{E}_i$, and $c_t = Cum_{\Delta c,t} = \sum_{i=1}^{t} \Delta c_i$, .

The state variable's dynamics is presented in Appendix A. This dynamics of Z_t can be concisely written in matrix form:

$$A_0^* Z_t = A_{1,t}^* Z_{t-1} + \omega_{0,t}^* + \omega_t^* W_t, \tag{II.2}$$

where:

$$A_0^* = \begin{bmatrix}
1 & 0 & \dots & & & & & & & & & & & \\
0 & 1 & 0 & \dots & & & & & & & & & & \\
0 & 0 & 1 & -1 & 0 & \dots & & & & & & & & \\
0 & 0 & 0 & 1 & 0 & \dots & & & & & & & & \\
 & & \dots & 0 & 1 & -\frac{\tau}{\log(2) M_{PI}(1+m_0)} & \dots & & & & & & & \\
 & & & \dots & 0 & 1 & 0 & \dots & & & & & & \\
 & & & & \dots & 0 & 1 & 0 & \dots & & & & & \\
 & & & & & \dots & 0 & 1 & 0 & \dots & & & & \\
0 & 0 & 0 & 0 & -\xi_1 & 0 & 0 & 0 & 1 & 0 & 0 & 0 & 0 & 0 \\
 & & & & & & & \dots & 0 & 1 & 0 & 0 & 0 & 0 \\
 & & & & & & & & \dots & 0 & 1 & 0 & 0 & 0 \\
0 & 0 & -1 & 0 & \dots & & & & & \dots & 0 & 1 & 0 & 0 \\
-1 & 0 & \dots & & & & & & & & \dots & 0 & 1 & 0 \\
0 & 0 & 0 & 0 & 0 & 0 & 0 & 0 & -\Delta t \times a_{SAT} - b_{SAT} & 0 & \dots & 0 & 0 & 1
\end{bmatrix},$$

$$A_{1,t}^* = \begin{bmatrix}
0 & \dots & & & & & & & & & & & & \\
0 & 1 & 0 & \dots & & & & & & & & & & \\
0 & 0 & 0 & \dots & & & & & & & & & & \\
0 & \kappa_t & 0 & 0 & \dots & & & & & & & & & \\
 & & & \dots & 0 & \dots & & & & & & & & \\
0 & 0 & \frac{\Delta t}{3.666} & 0 & 0 & \begin{bmatrix} \varphi_{11} & \varphi_{21} & 0 \\ \varphi_{12} & \varphi_{22} & \varphi_{32} \\ 0 & \varphi_{23} & \varphi_{33} \end{bmatrix}^{\Delta t} & & 0 & \dots & & & & & \\
 & & & \dots & 0 & & & 0 & \dots & & & & & \\
 & & & \dots & 0 & & & 0 & \dots & & & & & \\
 & & & & & & \dots & 0 & 1-\xi_1(\frac{\tau}{v}+\xi_2) & \xi_1\xi_2 & 0 & 0 & 0 & 0 \\
 & & & & & & \dots & 0 & \xi_3 & 1-\xi_3 & 0 & 0 & 0 & 0 \\
 & & & & & & & & \dots & 0 & -1 & 0 & 0 & 0 \\
 & & & & & & & & & \dots & 0 & 1 & 0 & 0 \\
 & & & & & & & & & & \dots & 0 & 1 & 0 \\
 & & & & & & \dots & 0 & -b_{SAT} & 0 & 0 & 0 & 0 & 1
\end{bmatrix},$$

and

$$\omega_{0,t}^* = \begin{bmatrix}
\mu_{c,t} \\
0 \\
\mathscr{E}_{Land,t} \\
\kappa_t \\
\frac{\tau}{\log(2)}\left[\log(1+m_0)-1\right] + F_{EX,t} \\
0 \\
0 \\
0 \\
0 \\
0 \\
0 \\
0 \\
0 \\
0 \\
-\Delta t \times a_{SAT} T_{0,S}
\end{bmatrix}, \quad \omega_t^* = \begin{bmatrix}
\sigma_{c,t} & 0 & 0 & -1 & 0 \\
\sigma_{c,t} & 0 & 0 & 0 & 0 \\
0 & 0 & 0 & 0 & 1 \\
0 & 0 & 0 & 0 & 0 \\
0 & \sigma_F & 0 & 0 & 0 \\
0 & 0 & 0 & 0 & 0 \\
0 & 0 & 0 & 0 & 0 \\
0 & 0 & 0 & 0 & 0 \\
0 & 0 & 0 & 0 & 0 \\
0 & 0 & 0 & 0 & 0 \\
0 & 0 & 0 & -1 & 0 \\
0 & 0 & 0 & 0 & 0 \\
0 & 0 & 0 & 0 & 0 \\
0 & 0 & \sigma_H & 0 & 0
\end{bmatrix}.$$

Pre-multiplying both sides of (II.2) by $(A_0^*)^{-1}$, we obtain:

$$Z_t = A_{1,t} Z_{t-1} + \omega_{0,t} + \omega_t W_t, \tag{II.3}$$

with

$$A_{1,t} = (A_0^*)^{-1} A_{1,t}^*, \quad \omega_{0,t} = (A_0^*)^{-1} \omega_{0,t}^*, \quad \omega_t = (A_0^*)^{-1} \omega_t^*.$$

II.2 Laplace transform of W_t

Proposition 1. *The Laplace transform of W_t, considering $u_W = [u_\eta', u_D, u_N]'$, is given by:*

$$\psi_W(u_W) := \mathbb{E}_t(\exp[u_W' W_{t+1}]) = \exp(\alpha_W(u_W) + \beta_W(u_W)' X_t) \quad \forall t, \tag{II.4}$$

with

$$\begin{cases} \alpha_W(u_W) &= \frac{u_\eta u_\eta'}{2} + \frac{u_D \mu_D}{1-u_D\mu_D} \ell_0^{(D)} + \frac{u_N \mu_N}{1-u_N\mu_N} \ell_0^{(N)} \\ \beta_W(u_W) &= \begin{bmatrix} 0_{14\times 1} \\ \Phi' u_\eta \\ 0_{2\times 1} \end{bmatrix} + \frac{u_D \mu_D}{1-u_D\mu_D} \ell_1^{(D)} + \frac{u_N \mu_N}{1-u_N\mu_N} \tilde{\ell}_1^{(N)}, \end{cases} \tag{II.5}$$

where vector $\tilde{\ell}_1^{(N)}$ is such that $\tilde{\ell}_1^{(N)\prime} X_t = \frac{\rho_N}{\mu_N} N_t + \ell_1^{(N)\prime} X_t$.

Proof. The shocks being conditionally independent, and using the Laplace transform of the gamma-zero distribution (Monfort et al., 2017) used to model D_t and N_t (see (28) and (29)), we have:

$$\begin{aligned} & \mathbb{E}_t\left(\exp\left(u_W' W_{t+1}\right)\right) = \mathbb{E}_t\left[\exp\left(u_\eta' \eta_{t+1} + u_D D_{t+1} + u_N N_{t+1}\right)\right] \\ = \; & \exp\left(u_\eta' \Phi \eta_t\right) \mathbb{E}_t\left(\exp\left(u_\eta' \varepsilon_{\eta,t+1}\right)\right) \mathbb{E}_t\left(\exp\left(u_D P_{D,t+1}\right)\right) \mathbb{E}_t\left(\exp\left(u_N P_{N,t+1}\right)\right) \\ = \; & \exp\left[u_\eta' \Phi \eta_t + \frac{u_\eta u_\eta'}{2} + \frac{u_D \mu_D}{1-u_D\mu_D}\left(\ell_0^{(D)} + \ell_1^{(D)\prime} X_t\right) + \frac{u_N \mu_N}{1-u_N\mu_N}\left(\ell_0^{(N)} + \tilde{\ell}_1^{(N)\prime} X_t\right)\right], \end{aligned}$$

which gives the result. □

II.3 Simple and multi-horizon Laplace transforms of $X_t = [Z_t', W_t']'$

In Proposition 2 and Corollary 1, we consider a linear combination of the components of X_{t+1}, namely $u' X_{t+1} = u_Z' Z_{t+1} + u_W' W_{t+1}$ (i.e. $u = [u_Z', u_W']'$).

Proposition 2. One-period-ahead Laplace transform of $X_t = [Z_t', W_t']'$. *We have:*

$$\psi_t(u) := \mathbb{E}_t(\exp(u' X_{t+1})) = \exp(\alpha_t(u) + \beta_t(u)' X_t),$$

with

$$\begin{cases} \alpha_t(u) &= u_Z' \omega_{0,t+1} + \alpha_W(u_W + \omega_{t+1}' u_Z) \\ \beta_t(u) &= \begin{bmatrix} A_{1,t+1}' u_Z \\ 0_{(n_\eta+2)\times 1} \end{bmatrix} + \beta_W(u_W + \omega_{t+1}' u_Z), \end{cases} \tag{II.6}$$

where functions α_W and β_W are defined by (II.5).

Proof. We have:

$$\begin{aligned}
& \mathbb{E}_t(\exp(u'X_{t+1})) = \mathbb{E}_t[\exp(u_Z'Z_{t+1} + u_W'W_{t+1})] \\
= \; & \mathbb{E}_t(\exp(u_Z'(A_{1,t+1}Z_t + \omega_{0,t+1} + \omega_{W,t+1}W_{t+1}) + u_W W_{t+1})) \\
= \; & \exp\left[u_Z'(A_{1,t+1}Z_t + \omega_{0,t+1})\right] \mathbb{E}_t\left[\exp\left(\{u_W' + u_Z'\omega_{t+1}\}W_{t+1}\right)\right] \\
= \; & \exp\left[u_Z'(A_{1,t+1}Z_t + \omega_{0,t+1}) + \alpha_W\left(u_W + \omega_{t+1}'u_Z\right) + \beta_W\left(u_W + \omega_{t+1}'u_Z\right)'X_t\right],
\end{aligned}$$

which gives the result. □

Proposition 3. Multi-horizon Laplace transform of $X_t = [Z_t', D_t]'$. *We have:*

$$\begin{aligned}
\psi_t^{(h)}(u_1,\ldots,u_h) &:= \mathbb{E}_t(\exp[u_1'X_{t+1} + \cdots + u_h'X_{t+h}) \\
&= \exp\left[\psi_{0,t}^{(h)}(u_1,\ldots,u_h) + \psi_{1,t}^{(h)}(u_1,\ldots,u_h)'X_t\right],
\end{aligned} \tag{II.7}$$

where, for all t and for $h > 1$:

$$\left\{\begin{array}{rcl}
\psi_{0,t}^{(h)}(u_1,\ldots,u_h) &=& \psi_{0,t+1}^{(h-1)}(u_2,\ldots,u_h) + \alpha_t\left(u_1 + \psi_{1,t+1}^{(h-1)}(u_2,\ldots,u_h)\right) \\
\psi_{1,t}^{(h)}(u_1,\ldots,u_h) &=& \beta_t\left(u_1 + \psi_{1,t+1}^{(h-1)}(u_2,\ldots,u_h)\right),
\end{array}\right. \tag{II.8}$$

and with, for all s, $\psi_{0,s}^{(1)}(u) = \alpha_s(u)$ and $\psi_{1,s}^{(1)}(u) = \beta_s(u)$, functions α_s and β_s being defined in (II.6).

In practice: *Using the notation $U_k = \psi_{1,t+h-k}^{(k)}(u_{h-k+1},\ldots,u_h)$ [with, notably, $U_h = \psi_{1,t}^{(h)}(u_1,\ldots,u_h)$], the second equation of (II.8) implies that, for $k \geq 2$:*

$$U_k = \beta_{t+h-k}(u_{h-k+1} + U_{k-1}),$$

which allows to compute the U_k ($k = 1,\ldots,h$) by backward recursions, starting from $U_1 = \beta_{t+h-1}(u_h)$. Once the U_k ($k = 1,\ldots,h$) are computed, the first equation of (II.8) gives $\psi_{0,t}^{(h)}(u_1,\ldots,u_h)$. Specifically, for $h \geq 1$, we have:

$$\psi_{0,t}^{(h)}(u_1,\ldots,u_h) = \alpha_t(u_1 + U_{h-1}) + \alpha_{t+1}(u_2 + U_{h-2}) + \cdots + \alpha_{t+h-2}(u_{h-1} + U_1) + \alpha_{t+h-1}(u_h).$$

Proof. We have:

$$\begin{aligned}
& \mathbb{E}_t(\exp[u_1'X_{t+1} + \cdots + u_h'X_{t+h}]) \\
= \; & \mathbb{E}_t\left(\mathbb{E}_{t+1}(\exp[u_1'X_{t+1} + \cdots + u_h'X_{t+h}])\right) \\
= \; & \mathbb{E}_t\left(\exp\left[u_1'X_{t+1} + \psi_{0,t+1}^{(h-1)}(u_2,\ldots,u_h) + \psi_{1,t+1}^{(h-1)}(u_2,\ldots,u_h)'X_{t+1}\right]\right) \\
= \; & \exp\left[\psi_{0,t+1}^{(h-1)}(u_2,\ldots,u_h) + \alpha_t\left(u_1 + \psi_{1,t+1}^{(h-1)}(u_2,\ldots,u_h)\right) + \beta_t\left(u_1 + \psi_{1,t+1}^{(h-1)}(u_2,\ldots,u_h)\right)'X_t\right],
\end{aligned}$$

which leads to the result by induction. □

Corollary 1. (Simple) multi-horizon Laplace transform of $X_t = [Z_t', D_t]'$. *Using the ψ notation introduced in Proposition 3 (via equation II.7), we have:*

$$\psi_t^{(h)}(0,\ldots,0,u) = \mathbb{E}_t(\exp(u'X_{t+h})) = \exp\left[a_{t,h}(u) + b_{t,h}(u)'X_t\right],$$

where $b_{t,k}(u) = \beta_t \circ \cdots \circ \beta_{t+k-1}(u)$, and

$$a_{t,h} = \alpha_{t+h-1}(u) + \alpha_{t+h-2}(b_{t+h-1,1}(u)) + \cdots + \alpha_{t+1}(b_{t+2,h-2}(u)) + \alpha_t(b_{t+1,h-1}(u)),$$

where functions α_s and β_s are defined in (II.6).

In practice: *Using the notation $U_k = \psi_{1,t+h-k}^{(k)}(0,\ldots,0,u)$ [with, notably, $U_h = \psi_{1,t}^{(h)}(0,\ldots,0,u) = b_{t,h}(u)$], the second equation of (II.8) implies that, for $k \geq 2$:*

$$U_k = \beta_{t+h-k}(U_{k-1}),$$

which allows to compute the U_k ($k = 1,\ldots,h$) by backward recursions, starting from $U_1 = \beta_{t+h-1}(u)$. Once the U_k ($k = 1,\ldots,h$) are computed, the first equation of (II.8) gives $a_{t,h}(u) = \psi_{0,t}^{(h)}(u_1,\ldots,u_h)$. Specifically, for $h \geq 1$, we have:

$$a_{t,h}(u) = \alpha_t(U_{h-1}) + \alpha_{t+1}(U_{h-2}) + \cdots + \alpha_{t+h-2}(U_1) + \alpha_{t+h-1}(u).$$

II.4 Conditional mean and variance of W_t

Proposition 4. *The conditional mean of W_{t+1}, given the information available at t, is given by:*

$$\mathbb{E}_t(W_{t+1}) = \alpha_W^{(1)} + \beta_W^{(1)} X_t, \tag{II.9}$$

where

$$\begin{cases} \alpha_W^{(1)} &= \begin{bmatrix} \mathbf{0}_{(n_Z+n_\eta)\times 1} \\ \mu_D \ell_0^{(D)} \\ \ell_0^{(N)} \end{bmatrix}, \\ \beta_W^{(1)} &= \begin{bmatrix} \mathbf{0}_{n_Z\times n_Z} & \mathbf{0}_{n_Z\times n_\eta} & \mathbf{0}_{n_Z\times 1} & \mathbf{0}_{n_Z\times 1} \\ \mathbf{0}_{n_\eta\times n_Z} & \Phi_{n_\eta\times n_\eta} & \mathbf{0}_{n_\eta\times 1} & \mathbf{0}_{n_\eta\times 1} \\ \mathbf{0}_{1\times n_Z} & \mathbf{0}_{1\times n_\eta} & 0 & 0 \\ \mathbf{0}_{1\times n_Z} & \mathbf{0}_{1\times n_\eta} & 0 & \rho_N \end{bmatrix} + \mu_D \begin{bmatrix} \mathbf{0}_{n_Z\times n_X} \\ \mathbf{0}_{n_\eta\times n_X} \\ \ell_1^{(D)\prime} \\ \mathbf{0}_{1\times n_X} \end{bmatrix} + \mu_N \begin{bmatrix} \mathbf{0}_{n_Z\times n_X} \\ \mathbf{0}_{n_\eta\times n_X} \\ \mathbf{0}_{1\times n_X} \\ \ell_1^{(N)\prime} \end{bmatrix}. \end{cases}$$

Proof. We have $W_t = [\eta_t', D_t, N_t]'$, where the dynamics of η, D_t and N_t are respectively defined by (27), (28), and (29). We have:

$$\mathbb{E}_t(W_{t+1}) = \mathbb{E}_t \begin{bmatrix} \Phi\eta_t + \varepsilon_{\eta,t+1} \\ D_{t+1} \\ N_{t+1} \end{bmatrix} = \begin{bmatrix} \Phi\eta_t \\ \mu_D\left(\ell_0^{(D)} + \ell_1^{(D)\prime} X_t\right) \\ \rho_N N_t + \mu_N\left(\ell_0^{(N)} + \ell_1^{(N)\prime} X_t\right) \end{bmatrix},$$

which gives the result. □

Proposition 5. *The conditional variance of W_{t+1}, given the information available at t, is given by:*

$$Vec\left(\mathbb{V}\mathrm{ar}_t(W_{t+1})\right) = \alpha_W^{(2)} + \beta_W^{(2)} X_t, \tag{II.10}$$

with

$$\begin{cases} \alpha_W^{(2)} &= Vec\left(\begin{bmatrix} \boldsymbol{Id}_{n_\eta \times n_\eta} & 0 & 0 \\ \mathbf{0}_{n_\eta \times n_\eta} & 2\mu_D^2 \ell_0^{(D)} & 0 \\ \mathbf{0}_{n_\eta \times n_\eta} & 0 & 2\mu_N^2 \ell_0^{(N)} \end{bmatrix}\right) \\ \beta_W^{(2)} &= Vec\left(\begin{bmatrix} \mathbf{0}_{n_\eta \times n_\eta} & 0 & 0 \\ \mathbf{0}_{n_\eta \times n_\eta} & 2\mu_D^2 & 0 \\ \mathbf{0}_{n_\eta \times n_\eta} & 0 & 0 \end{bmatrix}\right) \ell_1^{(D)\prime} + Vec\left(\begin{bmatrix} \mathbf{0}_{n_\eta \times n_\eta} & 0 & 0 \\ \mathbf{0}_{n_\eta \times n_\eta} & 0 & 0 \\ \mathbf{0}_{n_\eta \times n_\eta} & 0 & 2\mu_N^2 \end{bmatrix}\right) \tilde{\ell}_1^{(N)\prime}, \end{cases}$$

where $\tilde{\ell}_1^{(N)}$ is such that $\tilde{\ell}_1^{(N)\prime} X_t = \frac{\rho_N}{\mu_N} N_t + \ell_1^{(N)\prime} X_t$.

Proof. The shocks being conditionally independent, we have:

$$\begin{aligned} \mathbb{V}\mathrm{ar}_t\left(W_{t+1}\right) &= \begin{bmatrix} \mathbb{V}\mathrm{ar}_t(\eta_{t+1}) & 0 & 0 \\ 0 & \mathbb{V}\mathrm{ar}_t(D_{t+1}) & 0 \\ 0 & 0 & \mathbb{V}\mathrm{ar}_t(N_{t+1}) \end{bmatrix} \\ &= \begin{bmatrix} \mathbf{Id}_{n_\eta \times n_\eta} & 0 & 0 \\ \mathbf{0}_{n_\eta \times n_\eta} & 2\mu_D^2 \left(\ell_0^{(D)} + \ell_1^{(D)\prime} X_t\right) & 0 \\ \mathbf{0}_{n_\eta \times n_\eta} & 0 & 2\mu_N^2 \left(\frac{\rho_N}{\mu_N} N_t + \ell_0^{(N)} + \ell_1^{(N)\prime} X_t\right) \end{bmatrix}, \end{aligned}$$

which gives the result. □

II.5 Conditional mean and variance of $X_t = [Z_t', W_t']'$

Proposition 6. *The conditional mean of X_{t+h}, given the information available at t, is given by:*

$$\mathbb{E}_t(X_{t+h}) = \alpha_{t,h}^{(1)} + \beta_{t,h}^{(1)} X_t, \tag{II.11}$$

where

$$\begin{cases} \alpha_{t,h}^{(1)} &= \mu_{X,t+h-1} + \Phi_{X,t+h-1}\mu_{X,t+h-2} + \cdots + \Phi_{X,t+1}^{h-1}\mu_{X,t}, \\ \beta_{t,h}^{(1)} &= \Phi_{X,t+h-1}\Phi_{X,t+h-2}\ldots\Phi_{X,t}, \end{cases}$$

with

$$\begin{aligned}\mu_{X,t} &= \begin{bmatrix}\omega_{0,t+1}\\ \mathbf{0}_{n_W\times 1}\end{bmatrix} + \begin{bmatrix}\mathbf{0}_{n_Z\times n_Z} & \omega_{t+1}\\ \mathbf{0}_{n_W\times n_Z} & \boldsymbol{Id}_{n_W\times n_W}\end{bmatrix}\alpha_W^{(1)}, \quad \textit{and}\\ \Phi_{X,t} &= \begin{bmatrix}A_{1,t+1} & \mathbf{0}_{n_Z\times n_W}\\ \mathbf{0}_{n_W\times n_Z} & \mathbf{0}_{n_W\times n_W}\end{bmatrix} + \begin{bmatrix}\mathbf{0}_{n_Z\times n_Z} & \omega_{t+1}\\ \mathbf{0}_{n_W\times n_Z} & \boldsymbol{Id}_{n_W\times n_W}\end{bmatrix}\beta_W^{(1)}.\end{aligned}$$

Proof. Using (II.3), we have:

$$X_{t+1} = \begin{bmatrix} Z_{t+1}\\ W_{t+1}\end{bmatrix} = \begin{bmatrix} A_{1,t+1}Z_t + \omega_{0,t+1} + \omega_{t+1}W_{t+1}\\ W_{t+1}\end{bmatrix}, \tag{II.12}$$

and therefore

$$\mathbb{E}_t(X_{t+1}) = \begin{bmatrix}A_{1,t+1}Z_t + \omega_{0,t+1}\\ \mathbf{0}_{n_W\times 1}\end{bmatrix} + \begin{bmatrix}\mathbf{0}_{n_Z\times n_Z} & \omega_{t+1}\\ \mathbf{0}_{n_W\times n_Z} & \mathbf{Id}_{n_W\times n_W}\end{bmatrix}(\alpha_W^{(1)} + \beta_W^{(1)}X_t),$$

which gives the result for $h = 1$.

The law of iterated expectation implies that the conditional expectation $\mathbb{E}_t(X_{t+h})$ is given by:

$$\mathbb{E}_t(X_{t+h}) = \mu_{X,t+h-1} + \Phi_{X,t+h-1}\mathbb{E}_t(X_{t+h-1}),$$

which leads to the result. □

Proposition 7. *The conditional variance of X_{t+h}, given the information available at t, is given by:*

$$Vec\left(\mathbb{V}ar_t(X_{t+h})\right) = \alpha_{t,h}^{(2)} + \beta_{t,h}^{(2)}X_t, \tag{II.13}$$

where

$$\begin{cases}\alpha_{t,h}^{(2)} &= \alpha_{t+h-1,1}^{(2)} + \beta_{t+h-1,1}^{(2)}\alpha_{t,h-1}^{(1)} + \left(\beta_{t+h-1,1}^{(1)}\otimes\beta_{t+h-1,1}^{(1)}\right)\alpha_{t,h-1}^{(2)}\\ \beta_{t,h}^{(2)} &= \beta_{t+h-1,1}^{(2)}\beta_{t,h-1}^{(1)} + \left(\beta_{t+h-1,1}^{(1)}\otimes\beta_{t+h-1,1}^{(1)}\right)\beta_{t,h-1}^{(2)},\end{cases} \tag{II.14}$$

with

$$\begin{cases}\alpha_{s,1}^{(2)} &= \left(\Gamma_s\otimes\Gamma_s\right)\alpha_W^{(2)}\\ \beta_{s,1}^{(2)} &= \left(\Gamma_s\otimes\Gamma_s\right)\beta_W^{(2)},\end{cases} \tag{II.15}$$

where $\Gamma_s = \begin{bmatrix}\omega_{s+1}\\ \boldsymbol{Id}_{n_W\times n_W}\end{bmatrix}$.

Proof. Let us start with the case $h = 1$. Using (II.12), we have:

$$\mathbb{V}\mathrm{ar}_t(X_{t+1}) = \mathbb{V}\mathrm{ar}_t\left(\begin{bmatrix}\omega_{t+1}\\ \mathbf{Id}_{n_W\times n_W}\end{bmatrix}W_{t+1}\right) = \Gamma_t\mathbb{V}\mathrm{ar}_t(W_{t+1})\Gamma_{t+1}',$$

where $\mathbb{V}\text{ar}_t(W_{t+1})$ is given by (II.10). This implies that:

$$Vec\left(\mathbb{V}\text{ar}_t(X_{t+1})\right) = (\Gamma_{t+1}\otimes\Gamma_{t+1})Vec\left(\mathbb{V}\text{ar}_t(W_{t+1})\right) = (\Gamma_{t+1}\otimes\Gamma_{t+1})\left(\alpha_W^{(2)}+\beta_W^{(2)}X_t\right),$$

where the last equality is obtained by applying Proposition 5. This proves (II.13) for $h=1$ (using II.15). Let us make the inductive hypothesis that (II.13) holds for $h-1$. More precisely, assume that, for any date t:

$$\text{Vec}\left(\mathbb{V}ar_t(X_{t+h-1})\right) = \alpha_{t,h-1}^{(2)}+\beta_{t,h-1}^{(2)}X_t.$$

The law of total variance yields:

$$\mathbb{V}ar_t(X_{t+h}) = \mathbb{E}_t(\mathbb{V}ar_{t+h-1}(X_{t+h})) + \mathbb{V}ar_t(\mathbb{E}_{t+h-1}(X_{t+h})).$$

We get:

$$\begin{aligned}
\text{Vec}\left(\mathbb{V}ar_t(X_{t+h})\right) &= \mathbb{E}_t\Big(\underbrace{\alpha_{t+h-1,1}^{(2)}+\beta_{t+h-1,1}^{(2)}X_{t+h-1}}_{\text{using the inductive hypothesis}}\Big) + \text{Vec}\Big(\mathbb{V}ar_t\Big(\underbrace{\alpha_{t+h-1,1}^{(1)}+\beta_{t+h-1,1}^{(1)}X_{t+h-1}}_{\text{using (II.11)}}\Big)\Big)\\
&= \alpha_{t+h-1,1}^{(2)}+\beta_{t+h-1,1}^{(2)}\Big(\underbrace{\alpha_{t,h-1}^{(1)}+\beta_{t,h-1}^{(1)}X_t}_{\text{using (II.11)}}\Big) + \text{Vec}\Big(\beta_{t+h-1,1}^{(1)}\mathbb{V}ar_t(X_{t+h-1})\beta_{t+h-1,1}^{(1)\prime}\Big)\\
&= \alpha_{t+h-1,1}^{(2)}+\beta_{t+h-1,1}^{(2)}\alpha_{t,h-1}^{(1)}+\beta_{t+h-1,1}^{(2)}\beta_{t,h-1}^{(1)}X_t +\\
&\quad \left(\beta_{t+h-1,1}^{(1)}\otimes\beta_{t+h-1,1}^{(1)}\right)\text{Vec}\left(\mathbb{V}ar_t(X_{t+1})\right)\\
&= \alpha_{t+h-1,1}^{(2)}+\beta_{t+h-1,1}^{(2)}\alpha_{t,h-1}^{(1)}+\beta_{t+h-1,1}^{(2)}\beta_{t,h-1}^{(1)}X_t +\\
&\quad \left(\beta_{t+h-1,1}^{(1)}\otimes\beta_{t+h-1,1}^{(1)}\right)\left(\alpha_{t,h-1}^{(2)}+\beta_{t,h-1}^{(2)}X_t\right),
\end{aligned}$$

using (II.13) for $h=1$.

To summarize, we have shown that: (II.13) is satisfied for $h=1$, and we have shown that, if it is satisfied for $h-1$ (with $h\geq 2$), then it is also satisfied for h (see equation II.13). By induction, it comes that it is satisfied for any $h\geq 1$.

□

In practice, in order to use (II.14), we need:

- $\alpha_{t+k,1}^{(2)}$, $\beta_{t+k,1}^{(2)}$ for all k of interest, using (II.15);
- $\alpha_{t+k,1}^{(1)} \equiv \mu_{X,t+k}$, $\beta_{t+k,1}^{(1)} \equiv \Phi_{X,t+k}$ for all k of interest;
- $\alpha_{t,k}^{(1)}$, $\beta_{t,k}^{(1)}$ for all k of interest, using (II.11).

III Pricing

III.1 Solving for the s.d.f.

Proposition 8. *In the context described by A.3, i.e. under (38), (39) and (40), and if, for $t \geq t_0$:*

$$\mu_{u,0,t} \equiv \mu_{u,0},\ \mu_{u,1,t} \equiv \mu_{u,1},\ \mu_{c,0,t} \equiv \mu_{c,0},\ \mu_{c,1,t} \equiv \mu_{c,1},\ \alpha_t(\bullet) \equiv \alpha(\bullet) \text{ and } \beta_t(\bullet) \equiv \beta(\bullet),$$

then we have:

$$u_t = c_t + \mu_{u,0,t} + \mu'_{u,1,t} X_t, \tag{III.1}$$

where

$$\left\{ \begin{array}{rcl} \mu_{u,0,t} & = & \delta(\mu_{u,0,t+1} + \mu_{c,0,t+1}) + \\ & & \dfrac{\delta}{1-\gamma}\alpha_t\{(1-\gamma)(\mu_{u,1,t+1} + \mu_{c,1,t+1})\} \\ \mu_{u,1,t} & = & \dfrac{\delta}{1-\gamma}\beta_t\{(1-\gamma)(\mu_{u,1,t+1} + \mu_{c,1,t+1})\}, \end{array} \right. \tag{III.2}$$

and where, for $t \geq t_0$, $\mu_{u,1,t}$ solves:

$$\mu_{u,1} = \frac{\delta}{1-\gamma}\beta\{(1-\gamma)(\mu_{u,1} + \mu_{c,1})\}, \tag{III.3}$$

and $\mu_{u,0,t}$ satisfies:

$$\mu_{u,0} = \frac{\delta}{1-\delta}\mu_{c,0} + \frac{\delta}{1-\delta}\frac{1}{1-\gamma}\alpha\{(1-\gamma)(\mu_{u,1} + \mu_{c,1})\}. \tag{III.4}$$

Proof. We start by positing a specification for the log-utility of the form of (III.1). Our objective is to determine whether a utility of this form can satisfy (38), and the conditions that then have to be satisfied by $\mu_{u,0,t}$ and $\mu_{u,1,t}$. Under (III.1), we have:

$$\begin{array}{rcl} \mathbb{E}_t \exp\left[(1-\gamma)u_{t+1}\right] & = & \mathbb{E}_t \exp\left[(1-\gamma)(c_{t+1} + \mu_{u,0,t+1} + \mu'_{u,1,t+1}X_{t+1})\right] \\ & = & \mathbb{E}_t \exp\left[(1-\gamma)(c_t + \Delta c_{t+1} + \mu_{u,0,t+1} + \mu'_{u,1,t+1}X_{t+1})\right] \\ & = & \exp\left[(1-\gamma)(c_t + \mu_{u,0,t+1} + \mu_{c,0,t+1})\right] \times \\ & & \mathbb{E}_t \exp\left[(1-\gamma)(\mu_{u,1,t+1} + \mu_{c,1,t+1})'X_{t+1}\right] \\ & = & \exp\left[(1-\gamma)(c_t + \mu_{u,0,t+1} + \mu_{c,0,t+1})\right] \times \\ & & \exp\left[\alpha_t\{(1-\gamma)(\mu_{u,1,t+1} + \mu_{c,1,t+1})\} + \beta_t\{(1-\gamma)(\mu_{u,1,t+1} + \mu_{c,1,t+1})\}'X_t\right]. \end{array}$$

Substituting for $\mathbb{E}_t \exp\left[(1-\gamma)u_{t+1}\right]$ in (38) gives:

$$\begin{array}{rcl} u_t & = & c_t + \delta(\mu_{u,0,t+1} + \mu_{c,0,t+1}) + \\ & & \dfrac{\delta}{1-\gamma}\Big(\alpha_t\{(1-\gamma)(\mu_{u,1,t+1} + \mu_{c,1,t+1})\} + \beta_t\{(1-\gamma)(\mu_{u,1,t+1} + \mu_{c,1,t+1})\}'X_t\Big). \end{array}$$

Therefore, for u_t to be equal to $c_t + \mu_{u,0,t} + \mu'_{u,1,t}X_t$, we need to have (III.2).

Equations (III.3) and (III.4) are obtained by setting $\mu_{u,1} = \mu_{u,1,t} = \mu_{u,1,t+1}$ and $\mu_{u,0} = \mu_{u,0,t} = \mu_{u,0,t+1}$ in (III.2). □

In practice, we start by solving (III.3), which can be done by using the Gauss-Newton algorithm. [49]

[49] A very good approximation to the solution is obtained in a few iteration. A relevant starting value of the Gauss-Newton

This yields $\mu_{u,1}$. Then, we obtain $\mu_{u,0}$ by (III.4). Once $\mu_{u,0,t_0}$ $(=\mu_{u,0})$ and $\mu_{u,1,t_0}$ $(=\mu_{u,1})$ are known, one can deduce the previous $\mu_{u,i,t}$'s by backward computations. Specifically, knowing $\mu_{u,1,t+1}$, one can deduce $\mu_{u,1,t}$ by using the second equation of (III.2). And knowing $\mu_{u,0,t+1}$ and $\mu_{u,1,t+1}$, the first equation of (III.2) yields $\mu_{u,0,t}$.

Proposition 9. *We have:*

$$\mathscr{M}_{t,t+1} = \exp[-(\eta_{0,t} + \eta_{1,t}' X_t) + \pi_t' X_{t+1} \underbrace{-\alpha_t(\pi_t) - \beta_t(\pi_t)' X_t}_{=-\psi_t(\pi_t),\ \textit{see Prop. 2}}],$$

with

$$\left\{ \begin{array}{rcl} \pi_t &=& (1-\gamma)\mu_{u,1,t+1} - \gamma\mu_{c,1,t+1} \\ \eta_{0,t} &=& -\log\delta + \mu_{c,0,t+1} + \alpha_t\{(1-\gamma)(\mu_{u,1,t+1}+\mu_{c,1,t+1})\} - \alpha_t(\pi_t) \\ \eta_{1,t} &=& \beta_t\{(1-\gamma)(\mu_{u,1,t+1}+\mu_{c,1,t+1})\} - \beta_t(\pi_t), \end{array} \right. \tag{III.5}$$

where the (recursive) computation of $\mu_{u,1,t+1}$ results from Proposition 8.

The short-term risk-free rate, that is $-\log\mathbb{E}_t(\mathscr{M}_{t,t+1})$, is given by:

$$r_t = \eta_{0,t} + \eta_{1,t}' X_t.$$

Proof. When agents' preferences are as in (38), the s.d.f. is given by (e.g. Piazzesi and Schneider, 2007):

$$\mathscr{M}_{t,t+1} = \delta \left(\frac{C_{t+1}}{C_t}\right)^{-1} \frac{\exp[(1-\gamma)u_{t+1}]}{\mathbb{E}_t(\exp[(1-\gamma)u_{t+1}])}.$$

Therefore, we have:

$$\begin{array}{rcl} \log\mathscr{M}_{t,t+1} &=& \log\delta - \Delta c_{t+1} + (1-\gamma)u_{t+1} - \log\mathbb{E}_t(\exp[(1-\gamma)u_{t+1}]) \\ &=& \log\delta - \Delta c_{t+1} + (1-\gamma)(c_t + \Delta c_{t+1} + \mu_{u,0,t+1} + \mu_{u,1,t+1}' X_{t+1}) \\ && -(1-\gamma)(c_t + \mu_{u,0,t+1} + \mu_{c,0,t+1}) \\ && -\alpha_t\{(1-\gamma)(\mu_{u,1,t+1}+\mu_{c,1,t+1})\} - \beta_t\{(1-\gamma)(\mu_{u,1,t+1}+\mu_{c,1,t+1})\}' X_t \\ &=& \log\delta - \mu_{c,0,t+1} - \alpha_t\{(1-\gamma)(\mu_{u,1,t+1}+\mu_{c,1,t+1})\} \\ && + \Big((1-\gamma)\mu_{u,1,t+1} - \gamma\mu_{c,1,t+1}\Big)' X_{t+1} - \beta_t\{(1-\gamma)(\mu_{u,1,t+1}+\mu_{c,1,t+1})\}' X_t, \end{array}$$

which leads to the result. □

---

algorithm is obtained by replacing function β, in (III.3), by its first-order Taylor expansion around zero: using Prop. 2, it can be seen that, when u is small, we have that $\beta(u) \approx Mu$ where

$$M = \left[\begin{bmatrix} A_1' \\ \mathbf{0}_{n_W \times n_Z} \end{bmatrix} \quad \mathbf{0}_{n_X \times n_W} \right] + \left[\mathbf{0}_{n_X \times n_Z} \quad \begin{bmatrix} \mathbf{0}_{n_Z \times n_\eta} \\ \Phi' \\ \mathbf{0}_{(n_W - n_\eta)\times n_\eta} \end{bmatrix} \quad \mu_D \ell_1^{(D)} \quad \mu_N \tilde{\ell}_1^{(N)} \right] \cdot \begin{bmatrix} \mathbf{0}_{n_Z \times n_Z} & \mathbf{0}_{n_Z \times n_W} \\ \omega' & Id_{n_W \times n_W} \end{bmatrix}.$$

Replacing the non-linear function $\beta\{(1-\gamma)(\mu_{u,1}+\mu_{c,1})\}$ with its linearized version—that is $M\cdot\{(1-\gamma)(\mu_{u,1}+\mu_{c,1})\}$—in (III.3) yields the (approximated) solution: $\mu_{u,1}^0 = \delta(I-\delta M)^{-1}M\mu_{c,1}$. This vector $\mu_{u,1}^0$ turns out to be a relevant starting value for the Gauss-Newton algorithm.

Corollary 2. *In this economy, the maximum Sharpe ratio, between dates t and $t+1$ is given by (see Hansen and Jagannathan, 1991):*

$$maxSR_t = \sqrt{\frac{\exp(\alpha_t(2\pi_t) + \beta_t(2\pi_t)'X_t)}{\exp(2\alpha_t(\pi_t) + 2\beta_t(\pi_t)'X_t)} - 1}.$$

Proof. The maximum Sharpe ratio is given by:

$$\begin{aligned}\frac{\sqrt{\mathbb{V}ar_t(\mathcal{M}_{t,t+1})}}{\mathbb{E}_t(\mathcal{M}_{t,t+1})} &= \frac{\sqrt{\mathbb{V}ar_t(\exp(\pi_t X_{t+1}))}}{\mathbb{E}_t(\exp(\pi_t X_{t+1}))} = \frac{\sqrt{\mathbb{E}_t(\exp(2\pi_t X_{t+1})) - \mathbb{E}_t(\exp(\pi_t X_{t+1}))^2}}{\mathbb{E}_t(\exp(\pi_t X_{t+1}))} \\ &= \frac{\sqrt{\exp(\alpha_t(2\pi_t) + \beta_t(2\pi_t)'X_t) - \exp(2\alpha_t(\pi_t) + 2\beta_t(\pi_t)'X_t)}}{\exp(\alpha_t(\pi_t) + \beta_t(\pi_t)'X_t)},\end{aligned}$$

which gives the result. □

III.2 Asset pricing

Proposition 10. *Consider an asset whose payoff, settled on date $t+h$, is $\exp(\omega' X_{t+h})$. The date-t price of this asset is given by:*

$$\varphi_t^{(h)}(\omega) := \exp\left(\varphi_{0,t}^{(h)}(\omega) + \varphi_{1,t}^{(h)}(\omega)' X_t\right),$$

where

$$\left\{\begin{array}{rcl}\varphi_{0,t}^{(h)}(\omega) &=& -\eta_{0,t} - \alpha_t(\pi_t) - \cdots - \eta_{0,t+h-1} - \alpha_{t+h-1}(\pi_{t+h-1}) + \psi_{0,t}^{(h)}(u_1,\ldots,u_h) \\ \varphi_{1,t}^{(h)}(\omega) &=& -\eta_{1,t} - \beta_t(\pi_t) + \psi_{1,t}^{(h)}(u_1,\ldots,u_h),\end{array}\right. \tag{III.6}$$

where the $\eta_{0,t}$'s, the $\eta_{1,t}$'s and the π_t's are defined in (III.5), where functions $\psi_{0,t}^{(h)}$ and $\psi_{1,t}^{(h)}$ are defined in (II.8) and where:

$$u_k = \left\{\begin{array}{ll}-\eta_{1,t+k} - \beta_{t+k}(\pi_{t+k}) + \pi_{t+k-1} & for \quad k = 1,\ldots,h-1, \\ \pi_{t+k-1} + \omega & for \quad k = h.\end{array}\right. \tag{III.7}$$

Proof. The price of this asset is given by:

$$\begin{aligned}&\mathbb{E}_t\left(\mathcal{M}_{t,t+h}\exp(\omega' X_{t+h})\right) \\ =\ &\mathbb{E}_t\left\{\exp\left(-\left[\eta_{0,t} + \alpha_t(\pi_t) + \{\eta_{1,t} + \beta_t(\pi_t)\}' X_t\right]\right.\right. \\ &-\left[\eta_{0,t+1} + \alpha_{t+1}(\pi_{t+1}) + \{\eta_{1,t+1} + \beta_{t+1}(\pi_{t+1})\}' X_{t+1}\right] + \pi_t' X_{t+1} \\ &\cdots \\ &-\left[\eta_{0,t+h-1} + \alpha_{t+h-1}(\pi_{t+h-1}) + \{\eta_{1,t+h-1} + \beta_{t+h-1}(\pi_{t+h-1})\}' X_{t+h-1}\right] + \pi_{t+h-2}' X_{t+h-1} \\ &\left.\left.+\pi_{t+h-1}' X_{t+h} + \omega' X_{t+h}\right)\right\} \\ =\ &\exp(-\eta_{0,t} - \alpha_t(\pi_t) - \cdots - \eta_{0,t+h-1} - \alpha_{t+h-1}(\pi_{t+h-1}))\exp(-\{\eta_{1,t} + \beta_t(\pi_t)\}' X_t) \times \\ &\exp\left[\psi_{0,t}^{(h)}(u_1,\ldots,u_h) + \psi_{1,t}^{(h)}(u_1,\ldots,u_h)' X_t\right],\end{aligned}$$

where functions $\psi_{0,t}^{(h)}$ and $\psi_{1,t}^{(h)}$ are defined in (II.8) and the u_k's are given in (III.7). □

Corollary 3. *Consider an asset whose payoff, settled on date $t+h$, is $\omega' X_{t+h}$. The date-t price of this asset is:*

$$\widetilde{\varphi}_t^{(h)}(\omega) = \lim_{\varepsilon \to 0} \frac{\varphi_t^{(h)}(\varepsilon\omega) - \varphi_t^{(h)}(0)}{\varepsilon},$$

where the computation of $\widetilde{\varphi}_t^{(h)}(\omega)$ is given by Proposition 10.

Proof. The derivative of $\exp(x\omega' X_{t+h})$ w.r.t. x is $\omega' X_{t+h}\exp(x\omega' X_{t+h})$. Evaluated at $x=0$, this derivative is equal to $\omega' X_{t+h}$, which leads to the result. □

Corollary 4. *Consider the temperature-indexed bond defined in 2. Denote by ω_T the vector that is such that $T_t = \omega_T' X_t$. The date-t price of this TIB is:*

$$(1-\chi T_{t,h}^0)\varphi_t^{(h)}(0) + \chi\widetilde{\varphi}_t^{(h)}(\omega_T).$$

where the computation of $\varphi_t^{(h)}(0)$ and $\widetilde{\varphi}_t^{(h)}(\omega)$ are respectively given by Proposition 10 and Corollary 3.

Proposition 11. *Consider an asset whose payoff, settled on date $t+h$, is:*

$$\exp\left(\omega' X_{t+h}\right)\mathbb{1}_{\{a'X_{t+h}<b\}}.$$

The date-t price of this asset is given by:

$$\hat{\varphi}_t^{(h)}(\omega,a,b) = \frac{\varphi_t^{(h)}(\omega)}{2} - \frac{1}{\pi}\int_0^\infty \frac{Im[\varphi_t^{(h)}(\omega+iax)\exp(-ibx)]}{x}dx,$$

where $Im(x)$ denotes the imaginary part of x and where function $\varphi_t^{(h)}$ is defined in Proposition 10.

Proof. This is a direct application of Proposition 2 (equation 2.12) of Duffie et al. (2000). □

Corollary 5. *Consider an asset whose payoff, settled on date $t+h$, is:*

$$\omega' X_{t+h}\mathbb{1}_{\{a'X_{t+h}<b\}}.$$

The date-t price of this asset is:

$$\bar{\varphi}_t^{(h)}(\omega,a,b) = \lim_{\varepsilon \to 0} \frac{\varphi_t^{(h)}(\varepsilon\omega,a,b) - \varphi_t^{(h)}(0,a,b)}{\varepsilon},$$

where the computation of $\widetilde{\varphi}_t^{(h)}(\omega,a,b)$ is given by Proposition 11.

Proof. The proof is the same as that of Corollary 3. □

III.3 Social cost of carbon

This subsection describes the computation of the Social Cost of Carbon (SCC), as defined by eq. (43).

As shown by Proposition 8, with preferences defined by (38), we have:

$$u_t = \log(U_t) = c_t + \mu_{0,u,t} + \mu_{1,u,t}' X_t,$$

or

$$U_t = C_t \exp\left(\mu_{0,u,t} + \mu_{1,u,t}' X_t\right). \tag{III.8}$$

According to eq. (43), the SCC is given by:

$$SCC_t = -\frac{\partial U_t}{\partial M_{AT,t}} \Big/ \frac{\partial U_t}{\partial C_t}.$$

Given (III.8), we have $\partial U_t/\partial C_t = U_t/C_t$ and $\partial U_t/\partial M_{AT,t} = \mu_{1,u,t,6} U_t$ (because $M_{AT,t}$ is the 6^{th} component of X_t, see (II.1)). Therefore:

$$SCC_t = -\mu_{1,u,t,6} C_t, \tag{III.9}$$

In other words, agents are willing to accept an increase in $M_{AT,t}$ of one unit if they are given an extra consumption of $|\mu_{1,u,t,6}|C_t$.

According to the World Bank, from 2015 to 2019, global final consumption expenditures (C_0) were of \$299tr (299×10^{12}). Therefore, if $M_{AT,t}$ is expressed in GtC, the social cost of carbon, expressed in dollars per ton of carbon, is given by:

$$|\mu_{1,u,t,6}| \times 299 \times 10^{12}/10^9 = |\mu_{1,u,t,6}| \times 299\,000.$$

Our framework also offers closed-form formulas for expectations of future SCCs. Indeed, using eq. (III.9), we get:

$$\begin{aligned}
\mathbb{E}_t(SCC_{t+h}) &= |\mu_{1,u,t,6}|\mathbb{E}_t(\exp(c_{t+h})) \\
&= |\mu_{1,u,t,6}|C_0\mathbb{E}_t(\exp(Cum_{\Delta c,t+h})), \quad \text{where } Cum_{\Delta c,t+h} = \textstyle\sum_{i=1}^{t} \Delta c_i \\
&= |\mu_{1,u,t,6}|C_0\mathbb{E}_t(\exp(\omega_c' X_{t+h})),
\end{aligned}$$

where $\omega_c = [0,\ldots,0,1]'$ (see eq. II.1). This conditional expectation can be computed using Corollary 1.

Furthermore, since:

$$\mathbb{1}_{\{SCC_{t+h}<x\}} = \mathbb{1}_{\{|\mu_{1,u,t,6}|\exp(c_{t+h})<x\}} = \mathbb{1}_{\{|\mu_{1,u,t,6}|C_0\exp(\omega_c' X_{t+h})<x\}} = \mathbb{1}_{\left\{\omega_c' X_{t+h} < \log\left(\frac{x}{C_0|\mu_{1,u,t+h,6}|}\right)\right\}},$$

it comes that the cumulative distribution function of future SCCs can be obtained by Fourier analysis.

IV Additional results

IV.1 Relationship between carbon concentrations and radiative forcing

Following, e.g., Nordhaus (2017), we consider the following relationship between radiative forcing and carbon concentration:

$$F_t - F_{EX,t} = \tau \log_2\left(\frac{M_{AT,t}}{M_{PI}}\right) + \sigma_F \eta_{F,t}, \tag{IV.1}$$

where M_{PI} stands for preindustrial concentration of carbon in the atmosphere.

This formulation implies that τ corresponds to the increase in radiative forcing resulting from a doubling of atmospheric carbon concentration.

Linarizing (IV.1) at $\frac{M_{AT,t}}{M_{PI}} = m_0$ gives (6), that is:

$$F_t = \tau \log_2(m_0) + \frac{\tau}{\log(2) m_0}\left(\frac{M_{AT,t}}{M_{PI}} - m_0\right) + F_{EX,t} + \sigma_F \eta_{F,t}.$$

In order to optimize the range of values of atmospheric carbon masses for which the linearization will be relevant, we take a value of m_0 that is consistent with the average carbon concentrations that will prevail between 2020 and 2100. More precisely, we take $m_0 = \frac{\overline{M}_{AT}}{M_{PI}}$, where $\overline{M}_{AT}$ is the 2020-2100 average of carbon masses underlying the IPCC 4.5 and 6.0 scenarios.

Panel (a) of Figure IV.1 compares (IV.1) to its linearized version (6). Panel (b) shows the model-implied distribution of carbon concentrations for two future dates, 2050 and 2100. In Panel (a) of Figure IV.1, we also report 90% confidence intervals for the future pairs $(M_{AT,t+h}, F_{t+h} - F_{EX,t+h})$. Together, these two panels suggest that, for the most likely values of future carbon masses, the first-order approximation of (IV.1) is of good quality.

IV.2 Mitigation rate

Figure IV.1 displays our model-implied emission control rate μ_t (see Subsection 4.2, and more precisely eq. 14). For the sake of comparison, the figure also shows the emission control rate prevailing in the 2016 version of the DICE model (Nordhaus, 2017).

Figure IV.1. Relationship between radiative forcing and atmospheric carbon concentration

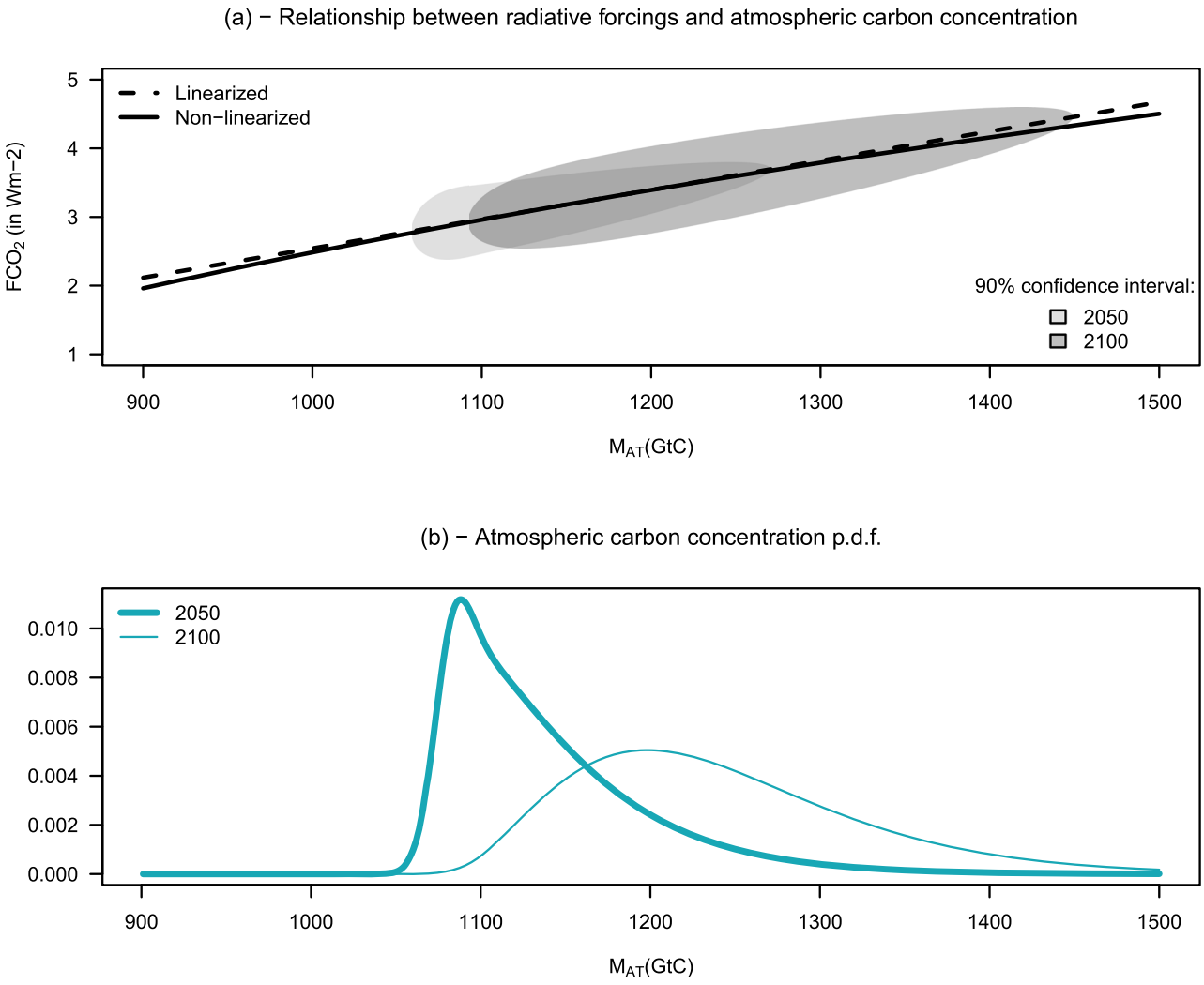

Note: This figure illustrates the quality of the first-order approximation of (IV.1). In Panel (a), the solid line (respectively the dashed line) represents the conditional expectation $\mathbb{E}(F_t - F_{EX,t}|M_{AT,t})$ resulting from the non-linear equation (IV.1) (resp. from the equation 6, that is its first-order approximation at m_0). Panel (b) displays the distributions of $M_{AT,t}$ for two dates t (2050 and 2100).

Figure IV.2. Mitigation rate

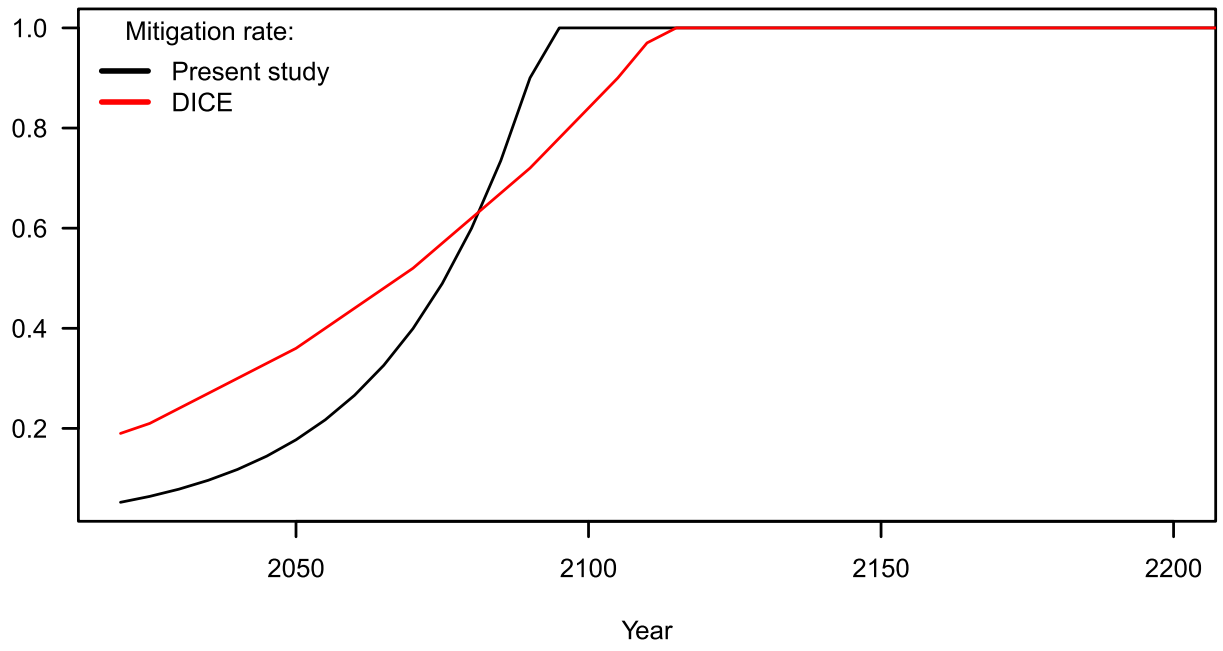

Note: This figure displays the mitigation rate (μ_t) underlying our baseline calibration (parametric representation 19). The red line represents the mitigation rate of the 2016 version of the DICE (Nordhaus, 2017).